

MACRO-LLM: LLM-Empowered Multi-Agent Collaborative Reasoning under Spatiotemporal Partial Observability

Handi Chen, Running Zhao*, Xiuzhe Wu*, Edith C.H. Ngai†,
The University of Hong Kong,

{hdchen, rnzhao}@connect.hku.hk {xzwu, chngai}@eee.hku.hk

Abstract

Large Language Model (LLM) agents deployed in complex real-world scenarios increasingly operate as spatially distributed entities. However, this physical dispersion constrains agents to limited local perception and finite temporal horizons. We characterize this bottleneck as spatiotemporal partial observability, where spatial and temporal limitations are fundamentally coupled: resolving spatial conflicts requires temporal reasoning about neighbors' future actions, while temporal planning requires spatial context beyond local perception. To bridge this gap, we introduce **MACRO-LLM**, LLM-empowered multi-agent collaborative reasoning under spatiotemporal partial observability. The architecture interleaves spatial and temporal reasoning within each decision cycle via three interdependent modules: (1) the CoProposer mitigates *temporal uncertainty* by verifying candidate actions via predictive rollouts; (2) the Negotiator overcomes *spatial myopia* by resolving conflicts through mean-field statistical aggregation, grounded in the CoProposer's rollout rewards; and (3) the Introspector closes the reasoning loop by analyzing environmental drift and attributing performance changes to refine strategies. Extensive evaluations on two complex long-horizon tasks, cooperative platoon planning and pandemic control, demonstrate that our framework enables robust coordination under spatiotemporal partial observability.

1 Introduction

Large Language Model (LLM) agents have demonstrated remarkable human-like capabilities in problem-solving (Zhu et al., 2023; Cui et al., 2025). While these agents successfully automate tasks across domains such as healthcare (Khasentino et al., 2025) and education (Zhao et al., 2025; Shi

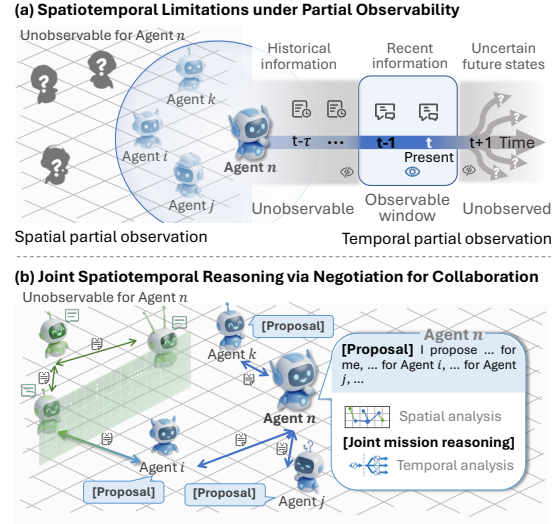


Figure 1: Illustration of spatiotemporal partial observability and the proposed collaborative reasoning framework. (a) Agents are constrained by limited local perception (spatial) and future uncertainty coupled with finite context windows (temporal). (b) Agents mitigate these limitations by exchanging proposals to establish collaborative framework via neighborhood negotiation.

et al., 2025), single agents often struggle with complexity and scalability in long-horizon scenarios. Inspired by the team collaboration in human societies, researchers are actively exploring systems where multiple LLM agents coordinate to achieve collective goals (Li et al., 2023a; Wang et al., 2024). This collective intelligence amplifies individual capabilities, enabling the effective resolution of complex reasoning tasks through coordination and negotiation (Zou et al., 2025). However, most existing frameworks assume shared global context or unrestricted communication among agents. As LLM agents increasingly operate in physical-world scenarios, coordination under limited local perception remains underexplored.

In such settings, agents operate as distributed entities (Chen et al., 2025), which inherently impose

*Equal contribution

†Corresponding author

spatiotemporal partial observability. Specifically, physical dispersion constrains agents to limited local perception, while the LLM’s fixed context window restricts their historical temporal information. This challenge is widespread: in pandemic control, districts must coordinate containment policies with only local infection data; in traffic coordination, vehicles optimize flow under communication limits and privacy constraints. Therefore, addressing the partial observability stemming from real-world distribution is pivotal for enhancing collaborative efficiency and effectiveness.

Specifically, partial observability manifests along two dimensions: *spatial* and *temporal*, as illustrated in Fig. 1(a). *Spatially*, constrained by communication limits and environmental complexity, each agent perceives only a fraction of the global information, preventing it from inferring the full context of the collective task. *Temporally*, the stochastic environment and unpredictable behaviors of others make long-term consequences difficult to predict, while finite historical context further hinders alignment of short-term decisions with long-term objectives. Together, these constraints result in suboptimal or even conflicting actions that degrade collective efficiency and effectiveness.

Existing LLM-based Multi-Agent Systems (MAS) aim to expand their spatial perception through inter-agent communication, as shown in Fig. 1 (b). This is typically implemented via hierarchical structures that aggregate information to a central node (Yu et al., 2024; Estornell et al., 2025) or fully-connected graphs that construct a pseudo-global view (Chan et al., 2023). However, these methods often incur communication bottlenecks at central nodes, limiting their scalability in large-scale, dynamically evolving environments. Temporally, while memory modules help mitigate limited historical observations (Park et al., 2023; Zhang et al., 2024), the inherent unpredictability of future states remains unaddressed. This uncertainty makes it difficult for agents to align immediate actions with long-term goals and capture cascading temporal effects. Prior to LLM-based MAS, Multi-Agent Reinforcement Learning (MARL) provides a traditional framework for partial observability but suffers from poor generalization and excessive training costs (Huh and Mohapatra, 2023), limiting its feasibility for complex real-world applications.

In this paper, we propose MACRO-LLM, an LLM-empowered multi-agent collaborative reasoning under spatiotemporal partial

observability, generalizable across diverse domains. A key insight is that spatial and temporal partial observability are *coupled*: resolving spatial conflicts requires predicting how neighbors will act in the future, while planning over time requires spatial context beyond local perception. Existing approaches address these dimensions in isolation. MACRO-LLM bridges this gap through a negotiation-centric architecture where spatial and temporal reasoning are interleaved within each decision cycle via three interdependent modules: the CoProposer, which generates collaborative proposals validated via predictive rollouts to mitigate temporal uncertainty; the Negotiator, which resolves conflicts through mean-field statistical aggregation of unobservable agents to overcome spatial myopia; and the Introspector, which refines strategies via scenario-aware adaptive reflection to ensure continuous adaptation. Our main contributions are summarized as follows:

Insightful. We explicitly decompose partial observability into spatial and temporal dimensions and address them jointly through a unified decentralized negotiation framework that couples semantic reasoning with mean-field statistical features, enabling robust long-horizon coordination without central coordinators or global views.

Technical. We develop MACRO-LLM with three interdependent modules forming a closed reasoning loop: the Negotiator’s confidence assessment consumes the CoProposer’s rollout rewards, and the Introspector’s revision signals reshape the strategies for subsequent cycles. This interdependence constitutes the core contribution beyond the individual techniques each module builds upon.

Experimental. We evaluate on two complementary domains, Cooperative Platoon Planning (CPP) and Pandemic Coordination (PC), covering continuous and discrete actions, linear and graph topologies, fine-grained and long-horizon planning. Results demonstrate MACRO-LLM’s superior coordination performance, scalability, and robustness across six LLM backbones.

2 Related Works

LLM-based Multi-Agent Systems. Existing LLM-based MAS have evolved from general collaboration frameworks (Li et al., 2023a; Wu et al., 2023) to structured systems with persistent memory and reasoning capabilities (Hong et al., 2023; Wang

et al., 2023). To address spatial partial observability, recent works adopt either *hierarchical aggregation*, which centralizes information flow (Yu et al., 2024; Estornell et al., 2025), or *belief-based inference*, which deduces hidden states via reasoning chains (Li et al., 2023b; Davidson et al., 2024). However, these approaches often rely on ideal communication bandwidth or static topologies, failing to account for the dynamic coupling of spatial dispersion and temporal uncertainty. Additionally, swarm-based optimization methods (Feng et al., 2024; Zhang et al., 2025) evolve agent configurations through offline iterative search, yielding static configurations that cannot adapt to runtime dynamics and lack coordination mechanisms for resolving conflicts under partial observability (see **Appendix A**). MACRO-LLM fills this gap by enabling decentralized spatiotemporal reasoning without reliance on central nodes or global views.

Multi-Agent Reinforcement Learning. Traditional approaches address partial observability via the Dec-POMDP framework (Oliehoek et al., 2016; Koops et al., 2024), often utilizing Centralized Training with Decentralized Execution (CTDE) (Kia et al., 2024; Bernstein et al., 2005) or Mean-Field approximations (Yang et al., 2018; Ganapathi Subramanian et al., 2020) to enhance scalability. While algorithms like MAPPO (Schulman et al., 2017), DMPO (Ma et al., 2024), and communication-aware methods like IC3Net (Singh et al., 2018) improve stability, they remain computationally intensive and environment-specific. They require costly retraining when transferring to new scenarios due to poor generalization (Huh and Mohapatra, 2023; Oroojlooy and Hajinezhad, 2023). In contrast, our framework leverages LLMs to achieve zero-shot generalization without parameter updates. Due to space constraints, we provide an extended review in **Appendix A**.

3 MACRO-LLM Framework

MACRO-LLM establishes a decentralized negotiation framework for MAS operating under spatiotemporal partial observability. As illustrated in Fig. 2, the architecture of agent n comprises three synergistic modules: (1) **CoProposer**, for collaborative proposal generation; (2) **Negotiator**, for conflict resolution and spatial strategy updates; and (3) **Introspector**, for temporal strategy refinement via scenario-aware adaptive reflection.

3.1 System Overview

We model the MAS as a peer-to-peer graph $\mathcal{G} = (\mathcal{V}, \mathcal{E})$, where \mathcal{V} denotes agents and \mathcal{E} communication links. For agent $n \in \mathcal{V}$, its neighborhood is $\mathcal{N}_n = \{m \in \mathcal{V} | (n, m) \in \mathcal{E}\}$. The system operates without a central coordinator. At initialization, each agent receives a system prompt defining the task, action space, state dynamics, and reward criteria. Architecturally, spatial and temporal reasoning are not separable. Evaluating an action requires predicting neighbors’ responses (temporal), but those predictions depend on unobservable states estimable only via mean-field spatial aggregation. MACRO-LLM operationalizes this dependency by interleaving the CoProposer and Negotiator within each negotiation round, with the Introspector providing cross-cycle feedback.

3.2 CoProposer

The CoProposer generates collaborative proposals P_n^t comprising actions for agent n and its observable neighbors \mathcal{N}_n by integrating long-term objectives with immediate spatial constraints.

Temporal Strategy Formulation. To align short-term decisions with global objectives despite incomplete information, we introduce a high-level temporal strategy. Agent n derives this strategy based on its current observation o_n^t , action space \mathcal{A}_n , and global objectives \mathcal{J}^{global} . This produces a macroscopic plan $\Pi_{n,t}^{temp} = \text{LLM}(o_n^t, \mathcal{A}_n, \mathcal{J}^{global})$, guiding step-by-step progression toward the goal.

Spatial Strategy Formulation. To incorporate spatial context, agent n infers potential cascading effects originating from unobservable agents. By analyzing its local observation o_n^t and the network topology \mathcal{G} , the agent forecasts multi-agent dynamics to formulate a spatial strategy $\Pi_{n,t}^{spatial}$.

Proposal Generation via Rollout-Simulated Verification. Leveraging current spatial and temporal strategies, agent n first generates an initial proposal $P_n^{t,0} = (o_n^t, a_n^{t,0}, \{a_{n \rightarrow m}^{t,0}\})$ by identifying the most advantageous action for itself and inferring cooperative actions for its neighbors \mathcal{N}_n . Due to future uncertainty, this proposal requires validation through rollout-simulated verification, performed via LLM inference without simulator access. Agent n predicts $\hat{o}_n^{t+1,0}$ by reasoning over domain dynamics, $\Pi_{n,t}^{temp}$, and $\Pi_{n,t}^{spatial}$, then assesses whether the predicted state constitutes an improvement. This process iterates over k steps, constituting a rollout.

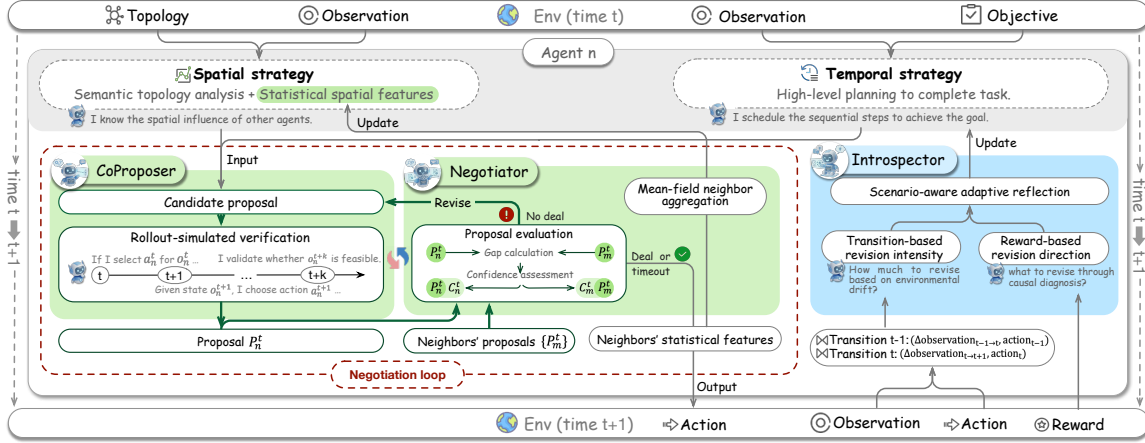


Figure 2: Architecture of MACRO-LLM for agent n . The framework comprises three synergistic modules: (1) the CoProposer generates proposals; (2) the Negotiator handles conflict resolution and spatial strategy updates; and (3) the Introspector performs strategy refinement. The CoProposer and Negotiator form a negotiation loop to process observations at time t and output coordinated actions, leading to the next observation at $t + 1$.

Rollout: In our framework, a rollout is a multi-step LLM-based projection from time t to $t + k$ that infers agent n 's future states and actions under its current strategy. The sequence of predicted observations, actions, and rewards across these k steps forms a trajectory, denoted as $\tau_n = ((o_n^t, a_n^t, R_n^t), \dots, (o_n^{t+k}, a_n^{t+k}, R_n^{t+k}))$.

To evaluate a rollout, we employ a progressive constraint relaxation mechanism. For the immediate step (t), the action must strictly satisfy all environmental constraints to ensure safety. For subsequent steps ($t+1$ to $t+k$), considering increasing uncertainty, criteria are relaxed to minimum viability constraints. This ensures the action a_n^t is safe while conducive to future positive outcomes. The estimated cumulative reward is formulated as:

$$\mathcal{R}(\tau_n) = \sum_{\iota=0}^k \gamma^\iota R_n(o_n^{t+\iota}, a_n^{t+\iota}). \quad (1)$$

To reduce computational complexity over long horizons, reward signals beyond $t+1$ are simplified to a binary indicator ($r = 1$ if constraints are met, else 0). If a proposal violates constraints during the rollout, agent n revises its proposed action until a valid proposal is found or the maximum attempt limit is reached. The candidate with the highest $\mathcal{R}(\tau_n)$ is selected and broadcast to neighbors. The pseudocode is provided in **Appendix B**.

3.3 Negotiator

In decentralized environments, agents generate proposals concurrently, inevitably introducing conflicts that necessitate a negotiation mechanism.

Neighborhood State Aggregation via Mean-Field Approximation. To extend agents' perception beyond observable limits, we complement semantic reasoning with statistical state features. In complex topologies, exchanging raw observations is inefficient due to bandwidth constraints. To address this, we introduce a protocol based on mean-field approximation to transmit aggregated statistical features.

The core idea of mean-field theory approximates complex pairwise interactions between an individual and all other agents in the environment by the interaction between the individual and an aggregated "mean field" effect (Lasry and Lions, 2007). Accordingly, we represent the neighborhood influence through weighted statistics. For an agent n , the state s_m^t of a neighbor m is decomposed into a local mean field and a fluctuation term:

$$s_m^t = \mu_n + \delta s_{n \rightarrow m}^t, \quad \mu_n = \frac{\sum_{m \in \mathcal{N}_n} w_{n,m} s_m^t}{\sum_{m \in \mathcal{N}_n} w_{n,m}}, \quad (2)$$

where μ_n represents the weighted mean of the neighborhood's spatial features. The weighted variance is defined as:

$$\sigma_n^2 = \frac{\sum_{m \in \mathcal{N}_n} w_{n,m} (s_m^t - \mu_n)^2}{\sum_{m \in \mathcal{N}_n} w_{n,m}}. \quad (3)$$

Here, weights $w_{n,m} > 0$ are determined by domain-specific relational factors, such as the spatial distance, relative speed between agents. During negotiation, agents transmit these statistical features instead of raw data to characterize unobservable contexts. Once agent n receives statistical features

(μ_m, σ_m^2, W_m) from a neighbor m , it updates the aggregated features incorporating its own state s_n^t (with weight w_n) using the weighted Welford algorithm (Welford, 1962). Since each neighbor already aggregates its own neighborhood’s states into the transmitted statistics, this enables agent n to incorporate spatial insights without requiring access to the raw states of all agents. The update equation is provided in **Appendix F**.

Eq. 1 defines the estimated cumulative reward $\mathcal{R}(\tau_n)$ for agent n ’s rollout trajectory τ_n . The trajectory τ_n depends on the neighborhood states $\mathbf{s}_{\mathcal{N}_n}^t = (s_1^t, \dots, s_{|\mathcal{N}_n|}^t)$, which influence the agent’s spatial strategy $\Pi_{n,t}^{\text{spatial}}$ (**Sec. 3.2**). Eq. 1 can be rewritten as $\mathcal{R}_n(\mathbf{s}_{\mathcal{N}_n}^t) \triangleq \mathcal{R}(\tau_n)$ to expose the neighborhood dependence. Therefore, the error is denoted as $|\mathcal{R}_n(\mathbf{s}_{\mathcal{N}_n}^t) - \mathcal{R}_n(\boldsymbol{\mu}_n)|$ i.e., the gap between the rollout reward computed with full neighborhood information $\mathbf{s}_{\mathcal{N}_n}^t$ and with the mean-field approximation $\boldsymbol{\mu}_n = (\mu_n, \dots, \mu_n)$.

To justify transmitting σ_n^2 as an approximation quality indicator, we invoke Eqs. (7)(8) and Appendix B of (Yang et al., 2018). In their formulation, pairwise Q-function interactions are approximated by the interaction with a mean agent, with the approximation error controlled by the variance of deviations from the mean. We apply the principle to analyze the theoretical properties of our mean-field aggregation, yielding the error bound:

$$|\mathcal{R}_n(\mathbf{s}_{\mathcal{N}_n}^t) - \mathcal{R}_n(\boldsymbol{\mu}_n)| \leq \frac{L_2}{2w_{\min}} \cdot \sigma_n^2, \quad (4)$$

where L_2 is a smoothness constant determined by the continuity of the underlying domain dynamics and the boundedness of the state-action spaces, which hold broadly in physically grounded environments with continuous dynamics and finite horizons (a detailed discussion is provided in **Appendix C**). σ_n^2 controls the approximation error bound. In many topologies, agent n acts as a cut vertex connecting disjoint subgroups (e.g., predecessor and follower in the CPP linear topology). Since these subgroups lack direct communication, their state distributions naturally diverge, making a single μ_n a poor summary. We prove that computing separate statistics per subgroup yields a provably tighter bound:

Theorem 1 (Tighter Bound via Topology-Aware Partitioning). *With the general error bound detailed in Eq. 4, computing separate weighted statistics per subgroup yields a tighter bound*

$$\begin{aligned} |\mathcal{R}_n(\mathbf{s}_{\mathcal{N}_n}^t) - \mathcal{R}_n(\boldsymbol{\mu}_n^{(1:P)})| &\leq \frac{L_2}{2w_{\min}} \sum_{p=1}^P |\mathcal{N}_n^{(p)}| \cdot \\ \sigma_n^{2,(p)} &\leq \frac{L_2}{2w_{\min}} \cdot |\mathcal{N}_n| \cdot \sigma_n^2. \end{aligned}$$

The proof is provided in **Appendix D**. Both bounds are controlled by σ_n^2 . Thus σ_n^2 serves a dual role: (1) *error indicator*: small σ_n^2 guarantees accurate mean-field approximation; (2) *uncertainty signal*: large σ_n^2 prompts conservative strategies. During negotiation, agents progressively align their strategies, reducing σ_n^2 and tightening both bounds over successive rounds.

Proposal Confidence Assessment and Regeneration. To evaluate proposal reliability, agent n computes the pairwise differences between its own proposal P_n^t and received neighbor proposals $\{P_m^t\}_{m \in \mathcal{N}_n}$. Local consensus between agents n and m is defined as $|P_n^{(q)} - P_m^{(q)}| < \delta$, where $\delta = \epsilon \cdot (a_{\max} - a_{\min})$ is proportional to the action space range for continuous actions, and $\delta = 0$ for discrete action spaces requiring exact agreement. If consensus is not met, the agent analyzes discrepancies, updates its spatial strategy by incorporating the received mean-field states, and integrates weighted neighbor proposals to regenerate a refined candidate, which then undergoes rollout verification as detailed in **Sec. 3.2**.

Multi-Round Negotiation. A complete iteration of the CoProposer (**Sec. 3.2**) and Negotiator (**Sec. 3.3**) constitutes a *negotiation round*. The primary purpose of multi-round negotiation is information propagation. Each round extends agents’ effective perception by one additional communication hop, with r rounds providing coverage of $r + 1$ hops. Local consensus serves as an early stopping criterion. Upon completion, agent n produces a final decision by weighting each neighbor’s proposal by the confidence scores from proposal evaluation, selecting the highest-confidence action (or weighted combination for continuous actions). We provide **Theorem 2**, which establishes that proposal quality is monotonically non-decreasing across rounds.

Theorem 2 (Properties of the Negotiation Loop). *Let \mathcal{G} be a connected graph and r be the maximum negotiation rounds. The negotiation loop satisfies:* (1) *Bounded Termination: The negotiation terminates in at most r rounds, either via early stopping when local consensus is reached ($\|P_n - P_m\| < \delta, \forall m \in \mathcal{N}_n$) or via the maximum round limit.* (2) *Monotonic Non-Decrease of Proposal Quality:*

$$\mathcal{R}(\tau_n^{(\ell+1)}) \geq \mathcal{R}(\tau_n^{(\ell)}), \quad \forall \ell = 0, 1, \dots, r-1.$$

The proof can be found in **Appendix E**. Regardless of whether agents reach consensus, the negotiation process terminates within r rounds, and proposal quality is guaranteed to be monotonically non-decreasing across rounds, exhibiting a convergent trend toward improved coordination.

3.4 Introspector

Due to spatiotemporal partial observability, an agent’s state inference is often compromised by dynamic environmental shifts and the unpredictable behaviors of others. Consequently, if an agent observes a reward decline between time steps, it initiates a self-reflection mechanism to update strategy. We model this process as *scenario-aware adaptive reflection*, which determines *how much* to revise based on environmental drift and *what* to revise through attribution-based reasoning.

Revision Intensity Estimation. We first quantify the magnitude of environmental shifts to determine the revision intensity. Let o_n^t denote the vectorized observation of agent n at time t . We construct a transition vector Γ_n^t by concatenating the min-max normalized observation difference and the action vector, defined as $\Gamma_n^t = (\Delta \tilde{o}_n^t, \tilde{a}_n^t)$, where $\Delta \tilde{o}_n^t = o_n^{t+1} - o_n^t$.

To evaluate scene consistency, we compute the cosine similarity between two consecutive transitions, Γ_n^{t-1} and Γ_n^t . The drift intensity (λ_{drift}) is derived from scene discontinuity:

$$\lambda_{\text{drift}} = 1 - \frac{\Gamma_n^{t-1} \cdot \Gamma_n^t}{\|\Gamma_n^{t-1}\| \cdot \|\Gamma_n^t\|}. \quad (5)$$

Higher λ_{drift} indicates greater environmental drift requiring aggressive revision, while lower values permit only fine-grained refinements. Combined with the reward-decline-based trigger condition to ensure genuine performance degradation.

Revision Direction Identification. We generate a *semantic revision signal* as a natural language description of the “direction” for strategic improvement. The LLM analyzes observation logs and negotiation records \mathbf{N}_t to identify which transitions deviated from the temporal strategy and to assess the impacts from neighbors. The revision signal $g_{n,t}^{\text{semantic}}$ is generated as textual rules that characterize the associations between actions, state changes, and negative reward outcomes, providing diagnostic guidance for strategy refinement.

Table 1: Performance comparison on the CPP task across *Catch-up* and *Slow-down* scenarios. Metrics include RMSE and SD for Headway (H) and Velocity (V). **Bold** and underline indicate best and second-best results, respectively.

Scenario 1: Catch-up				
Methods	RMSE-H (↓)	RMSE-V (↓)	SD-H (↓)	SD-V (↓)
ToM-Belief	5.514	4.409	4.002	3.130
ChatEval	5.495	2.113	2.947	1.241
LAMEN	1.891	0.648	3.320	0.601
DPPO	1.603	0.978	0.994	0.474
DMPO	4.765	0.534	3.025	1.349
IC3Net	8.687	4.205	7.232	3.399
MACRO-DS [†]	1.528	<u>0.553</u>	<u>0.611</u>	0.190
MACRO-Llama [†]	<u>1.412</u>	0.779	0.645	0.365
MACRO-GPT [†]	1.237	0.721	0.409	<u>0.203</u>
Scenario 2: Slow-down				
Methods	RMSE-H (↓)	RMSE-V (↓)	SD-H (↓)	SD-V (↓)
ToM-Belief	<u>0.641</u>	4.681	<u>0.225</u>	0.480
ChatEval	3.062	5.708	0.778	1.016
LAMEN	0.923	3.385	0.635	0.750
DPPO	1.720	<u>3.121</u>	1.410	1.176
DMPO	2.226	3.059	1.742	1.189
IC3Net	7.877	4.678	5.207	2.319
MACRO-DS [†]	0.649	3.388	0.274	<u>0.417</u>
MACRO-Llama [†]	1.163	3.736	0.889	1.224
MACRO-GPT [†]	0.496	3.310	0.128	0.238

[†] MACRO-X: DS denotes DeepSeek-V3.1, Llama denotes Llama-3.3-70B-Instruct, and GPT denotes GPT-4o.

Strategy Update. Finally, we update the temporal strategy using the revision signal and drift intensity. A concrete prompt template for strategy update with revision intensity and direction is provided in **Appendix Q.3**. The update is formulated as $\Pi_{n,t+1}^{\text{temp}} \leftarrow \text{LLM}(\Pi_{n,t}^{\text{temp}}, g_{n,t}^{\text{semantic}}, \lambda_{\text{drift}})$. The drift intensity λ_{drift} modulates the revision scope: a high λ_{drift} indicates substantial environmental drift, instructing the LLM to aggressively revise the strategy according to $g_{n,t}^{\text{semantic}}$; a low λ_{drift} confines revision to fine-grained adjustments, preserving the core of the existing strategy $\Pi_{n,t}^{\text{temp}}$.

4 Experiments

4.1 Experimental Settings

Task Configurations. We evaluate MACRO-LLM across two complementary tasks where coordination outcomes are measured through domain-specific physical metrics, ensuring that performance gains reflect genuine coordination ability rather than language fluency. (1) *Cooperative Platoon Planning (CPP)* (Chu et al., 2020): a multi-agent vehicle platooning task (default N=8) with dynamic “Catch-up” and “Slow-down” scenarios. (2) *Pandemic Control (PC)* (Kompella* et al., 2020): a strategic planning task where agents select regulation level to mitigate virus spread across

three urban topologies (Helsinki, Hong Kong, and New York). CPP and PC tasks span continuous and discrete action spaces, linear and mixed topologies, and fine-grained and long-horizon decision-making, respectively. Refer to **Appendix G** for simulator configurations and city topologies.

Implementation Details. We implement MACRO-LLM as a backbone-agnostic framework and evaluate it across six LLM backbones: GPT-4o, GPT-4o-mini, DeepSeek-V3.1, Llama-3.3-70B-Instruct, Mistral-Small-3.2-24B-Instruct, and Qwen3-flash. Tables 1 and 2 report three representative backbones; the full generalizability analysis is in **Appendix K**. Scalability, ablation, and robustness analyses use GPT-4o as the default. Framework and task configurations are detailed in **Appendix G**. Results for MACRO-LLM are averaged over 5 independent runs; variance analysis confirming low standard deviations across all metrics is provided in **Appendix N**. A case study on hierarchical deployment with different LLM invocation frequency is in **Appendix I**.

Baselines. We benchmark MACRO-LLM against representative methods from two paradigms: (1) *LLM-based MAS baselines*, which share the same backbone (GPT-4o) and environmental interfaces to provide controlled comparisons: ToM-Belief (Li et al., 2023b), ChatEval (Chan et al., 2023), and LAMEN (Davidson et al., 2024); and (2) *MARL baselines*, which serve as task-specialized performance references trained on each topology: DPPO, DMPO (Ma et al., 2024), and IC3Net (Singh et al., 2018). Details on baseline implementations, prompt adaptations, and the division between LLM reasoning and external numerical modules are provided in **Appendix H.3**.

Evaluation Metrics. For the CPP task, we evaluate platoon stability via the Root Mean Square Error (RMSE) and Standard Deviation (SD) of both velocity and headway distance (denoted as RMSE-V/H and SD-V/H). For the PC task, we assess containment efficacy through Normalized Infection (I_n), Peak Infection (PI_n), Normalized Death (D_n) and total Pandemic Duration (PD). Metric definitions are detailed in **Appendix J**.

4.2 Performance of Cooperative Platoon Planning Task

As shown in Table 1, MACRO-LLM consistently outperforms both MARL and LLM-based base-

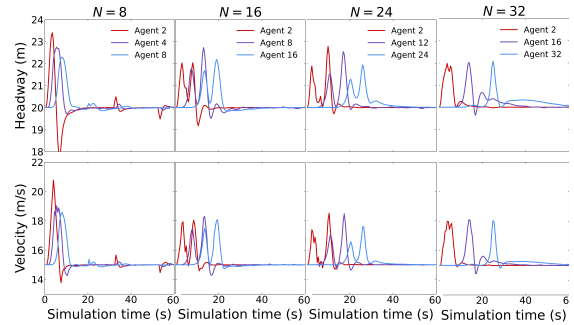


Figure 3: Scalability analysis of MACRO-LLM on the CPP task for number of agents $N \in \{8, 16, 24, 32\}$.

lines across multiple backbones. In the *Catch-up* scenario, all three MACRO-LLM variants achieve the top RMSE-H and SD-H results. The SD-H of MACRO-GPT (0.409 ± 0.034 , **Appendix N**) is 87.7% lower than that of LAMEN and 58.9% lower than that of DPPO, while even MACRO-DS attains lower SD-H than all baselines. In the *Slow-down* scenario, MACRO-LLM prioritizes headway safety over aggressive velocity matching. MACRO-GPT achieves the lowest SD-H (0.128 ± 0.054 , **Appendix N**), a 43.1% improvement over ToM-Belief, while maintaining competitive velocity errors. The consistent advantage across three diverse backbones confirms that the performance gains stem from the framework’s negotiation mechanism rather than any single model’s capability.

4.3 Performance on Pandemic Control Task.

Table 2 presents the comparative results across three city topologies. MACRO-LLM consistently achieves the lowest infection rates and shortest pandemic durations across all settings. In *New York* topology, all three MACRO-LLM variants reduce cumulative infections by over 99% compared to DPPO while shortening the pandemic duration from 95 to as few as 11 days (MACRO-DS). In *Hong Kong*, MACRO-Llama reduces PD to 16 days, outperforming LAMEN (23 days) at comparable infection levels. MACRO-LLM achieves both low infections and short durations simultaneously. This consistent advantage across three diverse backbones confirms that the coordination gains stem from the framework’s negotiation mechanism rather than any single model’s capability.

4.4 Analysis of Scalability

To investigate scalability, we extend the CPP Catch-up scenario to fleet sizes $N \in \{8, 16, 24, 32\}$. As illustrated in Fig. 3, MACRO-LLM maintains

Table 2: Performance comparison on the PC task across Helsinki, Hong Kong, and New York topologies. Metrics include Normalized Infection (I_n), Peak Infection (PI_n), Normalized Death (D_n), and Pandemic Duration (PD). **Bold** and underline indicate best and second-best results, respectively.

Methods	Helsinki				HongKong				NewYork			
	I_n (↓)	PI_n (↓)	D_n (↓)	PD (↓)	I_n (↓)	PI_n (↓)	D_n (↓)	PD (↓)	I_n (↓)	PI_n (↓)	D_n (↓)	PD (↓)
ToM-Belief	0.184	0.042	0.002	92	0.239	0.028	0.003	120	0.130	0.023	<u>0.001</u>	60
ChatEval	0.010	0.008	0.000	42	<u>0.009</u>	0.003	<u>0.001</u>	24	0.290	0.043	0.002	83
LAMEN	0.010	0.008	0.002	17	0.012	0.005	0.000	23	0.164	0.025	0.002	52
DPPO	0.426	0.110	0.007	62	0.370	0.083	0.004	83	0.923	0.363	0.009	95
DMPO	0.010	0.008	<u>0.001</u>	<u>13</u>	0.271	0.057	0.003	59	0.332	0.109	0.002	53
IC3Net	0.651	0.186	0.009	69	0.259	0.067	0.003	52	0.789	0.284	0.007	93
MACRO-DS [†]	0.098	<u>0.038</u>	0.002	46	0.008	0.005	<u>0.001</u>	<u>22</u>	0.003	0.003	0.000	11
MACRO-Llama [†]	0.013	0.008	0.000	14	0.012	0.005	0.000	16	0.013	<u>0.006</u>	0.000	<u>25</u>
MACRO-GPT [†]	<u>0.011</u>	0.008	0.000	10	0.008	<u>0.004</u>	<u>0.001</u>	23	<u>0.004</u>	0.003	0.000	<u>25</u>

[†] MACRO-X: DS denotes DeepSeek-V3.1, Llama denotes Llama-3.3-70B-Instruct, and GPT denotes GPT-4o.

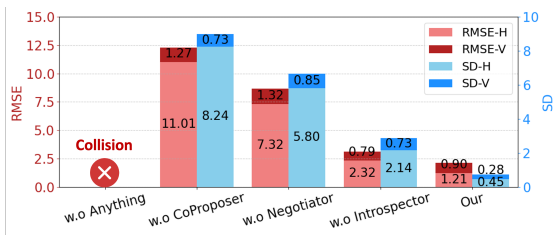


Figure 4: Ablation of MACRO-LLM—impact of each module on CPP performance.

consistent robustness as the network quadruples. Oscillation amplitudes remain bounded and all agents converge to the target equilibrium within 40s regardless of fleet size. Aggregated metrics (**Appendix L**, Table 6) reveal two complementary trends: RMSE-H decreases from 1.237 ($N=8$) to 0.728 ($N=32$), as the growing proportion of already-stabilized agents dilutes the transient deviations of those still responding to propagation. Meanwhile, SD-H increases moderately from 0.409 to 0.433, reflecting the inherently longer synchronization lag in larger platoons. Importantly, this increase is bounded. At $N=32$, SD-H remains 56.4% lower than that of DPPO ($N=8$), confirming that MACRO-LLM compresses large-scale interactions while ensuring coordination quality. Further scalability analyses are provided in **Appendix L**.

4.5 Ablation Study

We validate each module’s contribution in Figs. 4 and 5. Ablating the Negotiator degrades stability metrics drastically. Without the Introspector, agents fail to suppress oscillations over time. Notably, the ablations reveal cross-module dependencies: removing the CoProposer disables not only temporal verification but also the Negotiator’s confidence assessment without rollout rewards. It ex-

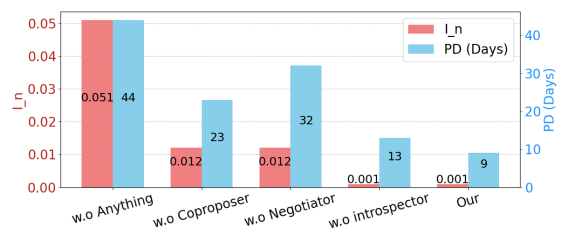


Figure 5: Ablation of MACRO-LLM—impact of each module on PC performance.

plains the largest SD-H degradation among all variants. Quantitative analyses are in **Appendix M**.

5 Conclusion

In this work, we present MACRO-LLM, a novel framework enabling agents to reason and coordinate through localized negotiations under spatiotemporal partial observability. We explicitly address the coordination challenge along spatial and temporal dimensions, addressing them through three interdependent modules: (1) a CoProposer to generate collaborative actions and mitigate future uncertainty via predictive rollouts; (2) a Negotiator that resolves spatial conflicts using mean-field statistical estimations; and (3) an Introspector that facilitates strategic refinement via scenario-aware adaptive reflection. Extensive experiments on CPP and PC tasks demonstrate MACRO-LLM’s capability to align local actions with long-term global objectives, achieving superior collaborative efficiency compared to representative baselines. Ultimately, our work highlights the critical role of explicitly modeling spatiotemporal dynamics in scaling LLM-based MAS.

Limitations

While MACRO-LLM demonstrates robust coordination capabilities, we acknowledge two primary limitations. First, as a strategic-level reasoning framework, MACRO-LLM’s iterative negotiation mechanism prioritizes decision quality over inference speed. The per-step latency is dominated by API network overhead of remote LLM calls, which is orthogonal to the framework’s reasoning complexity and can be mitigated through two composable strategies already validated in our experiments: (1) hierarchical deployment, where MACRO-LLM issues strategic directives every Δ steps while a lightweight controller maintains millisecond-level safety guarantees. Empirical results confirm that even with 90% fewer LLM invocations, coordination quality surpasses all baselines (**Appendix I**, Table 4); and (2) local deployment of lightweight models such as Qwen-flash and Mistral-small-3.2-24B-Instruct, which eliminates API latency entirely while maintaining competitive performance (**Appendix K**). Future work will explore tighter co-design between the strategic layer and domain-specific execution layers to further optimize the reasoning-latency balance. Second, relying on foundation models requires additional context injection for domain adaptation, which increases token consumption. Future work will explore online self-evolution mechanisms, such as experience-driven prompt distillation and adaptive strategy caching, that enable agents to progressively internalize domain-specific knowledge through interaction, reducing context dependency while improving cross-domain adaptability.

References

- Emile Anand, Ishani Karmarkar, and Guannan Qu. 2024. Mean-field sampling for cooperative multi-agent reinforcement learning. *CoRR*.
- Jinze Bai, Shuai Bai, Yunfei Chu, Zeyu Cui, Kai Dang, Xiaodong Deng, Yang Fan, Wenbin Ge, Yu Han, Fei Huang, and 1 others. 2023. Qwen technical report. *arXiv preprint arXiv:2309.16609*.
- Daniel S Bernstein, Eric A Hansen, and Shlomo Zilberstein. 2005. Bounded policy iteration for decentralized pomdps. In *Proceedings of the nineteenth international joint conference on artificial intelligence (IJCAI)*, pages 52–57.
- Maciej Besta, Nils Blach, Ales Kubicek, Robert Gerstenberger, Michal Podstawski, Lukas Gianinazzi, Joanna Gajda, Tomasz Lehmann, Hubert Niewiadomski, Piotr Nyczyk, and 1 others. 2024. Graph of thoughts: Solving elaborate problems with large language models. In *Proceedings of the AAAI conference on artificial intelligence*, volume 38, pages 17682–17690.
- George Casella and Roger Berger. 2024. *Statistical inference*. Chapman and Hall/CRC.
- Chi-Min Chan, Weize Chen, Yusheng Su, Jianxuan Yu, Wei Xue, Shanghang Zhang, Jie Fu, and Zhiyuan Liu. 2023. Chateval: Towards better llm-based evaluators through multi-agent debate. *International Conference on Learning Representations*.
- Tony F Chan, Gene H Golub, and Randall J LeVeque. 1983. Algorithms for computing the sample variance: Analysis and recommendations. *The American Statistician*, 37(3):242–247.
- Handi Chen, Weipeng Deng, Shuo Yang, Jinfeng Xu, Zhihan Jiang, Edith C. H. Ngai, Jiangchuan Liu, and Xue Liu. 2025. [Toward edge general intelligence via large language models: Opportunities and challenges](#). *IEEE Network*, 39(5):263–271.
- Tianshu Chu, Sandeep Chinchali, and Sachin Katti. 2020. Multi-agent reinforcement learning for networked system control. *International Conference on Learning Representations*.
- Hao Cui, Zahra Shamsi, Gowoon Cheon, Xuejian Ma, Shutong Li, Maria Tikhanovskaya, Peter Christian Norgaard, Nayantara Mudur, Martyna Beata Plomecka, Paul Raccuglia, Yasaman Bahri, Victor V. Albert, Pranesh Srinivasan, Haining Pan, Philippe Faist, Brian A Rohr, Michael J. Statt, Dan Morris, Drew Purves, and 11 others. 2025. [CURIE: Evaluating LLMs on multitask scientific long-context understanding and reasoning](#). In *The Thirteenth International Conference on Learning Representations*.
- Tim R Davidson, Veniamin Veselovsky, Martin Josifoski, Maxime Peyrard, Antoine Bosselut, Michal Kosinski, and Robert West. 2024. Evaluating language model agency through negotiations. *International Conference on Learning Representations*.
- Charles Desjardins and Brahim Chaib-draa. 2011. [Cooperative adaptive cruise control: A reinforcement learning approach](#). *IEEE Transactions on Intelligent Transportation Systems*, 12(4):1248–1260.
- Andrew Estornell, Jean-Francois Ton, Muhammad Faaiz Taufiq, and Hang Li. 2025. How to train a leader: Hierarchical reasoning in multi-agent llms. *arXiv preprint arXiv:2507.08960*.
- Shangbin Feng, Zifeng Wang, Yike Wang, Sayna Ebrahimi, Hamid Palangi, Lesly Miculicich, Achin Kulshrestha, Nathalie Rauschmayr, Yejin Choi, Yulia Tsvetkov, and 1 others. 2024. Model swarms: Collaborative search to adapt llm experts via swarm intelligence. *Proceedings of the International Conference on Machine Learning*.
- Sriram Ganapathi Subramanian, Pascal Poupart, Matthew E Taylor, and Nidhi Hegde. 2020. Multi type mean field reinforcement learning. In *Proceedings of the 19th International Conference on Autonomous Agents and MultiAgent Systems*, pages 411–419.
- Aaron Grattafiori, Abhimanyu Dubey, Abhinav Jauhri, Abhinav Pandey, Abhishek Kadian, Ahmad Al-Dahle, Aiesha Letman, Akhil Mathur, Alan Schelten, Alex Vaughan, and 1 others. 2024. The llama 3 herd of models. *arXiv preprint arXiv:2407.21783*.
- Haotian Gu, Xin Guo, Xiaoli Wei, and Renyuan Xu. 2025. Mean-field multiagent reinforcement learning: A decentralized network approach. *Mathematics of Operations Research*, 50(1):506–536.
- Sirui Hong, Mingchen Zhuge, Jonathan Chen, Xiawu Zheng, Yuheng Cheng, Jinlin Wang, Ceyao Zhang, Zili Wang, Steven Ka Shing Yau, Zijuan Lin, and 1 others. 2023. Metagpt: Meta programming for a multi-agent collaborative framework. In *The Twelfth International Conference on Learning Representations*.
- Zhipeng Hou, Junyi Tang, and Yipeng Wang. 2025. Halo: Hierarchical autonomous logic-oriented orchestration for multi-agent llm systems. *arXiv preprint arXiv:2505.13516*.
- Xu Huang, Weiwen Liu, Xiaolong Chen, Xingmei Wang, Hao Wang, Defu Lian, Yasheng Wang, Ruiming Tang, and Enhong Chen. 2024. Understanding the planning of llm agents: A survey. *arXiv preprint arXiv:2402.02716*.
- Dom Huh and Prasant Mohapatra. 2023. Multi-agent reinforcement learning: A comprehensive survey. *arXiv preprint arXiv:2312.10256*.
- Justin Khasentino, Anastasiya Belyaeva, Xin Liu, Zhun Yang, Nicholas A Furlotte, Chace Lee, Erik Schenck, Yojan Patel, Jian Cui, Logan Douglas Schneider, and 1 others. 2025. A personal health large language model for sleep and fitness coaching. *Nature Medicine*, pages 1–10.

- Maryam Kia, Jordan Cramer, and Artur Luczak. 2024. Memory augmented multi-agent reinforcement learning for cooperative environment. In *International Conference on Artificial Intelligence and Soft Computing*, pages 92–103. Springer.
- Varun Kompella*, Roberto Capobianco*, Stacy Jong, Jonathan Browne, Spencer Fox, Lauren Meyers, Peter Wurman, and Peter Stone. 2020. [Reinforcement learning for optimization of covid-19 mitigation policies](#). Preprint, arXiv:2010.10560.
- Wietze Koops, Sebastian Junges, and Nils Jansen. 2024. Approximate dec-pomdp solving using multi-agent a. In *Proceedings of the Thirty-Third International Joint Conference on Artificial Intelligence*, pages 6743–6751.
- Jean-Michel Lasry and Pierre-Louis Lions. 2007. Mean field games. *Japanese journal of mathematics*, 2(1):229–260.
- Chenfei Li, Yujia Liang, Zihan Song, and 1 others. 2023a. [Camel: Communicative agents for “mind” exploration of large language model society](#). arXiv preprint arXiv:2303.17760.
- Huaoli Li, Yu Quan Chong, Simon Stepputtis, Joseph Campbell, Dana Hughes, Michael Lewis, and Katia Sycara. 2023b. Theory of mind for multi-agent collaboration via large language models. *Empirical Methods in Natural Language Processing*.
- Aixin Liu, Bei Feng, Bing Xue, Bingxuan Wang, Bochao Wu, Chengda Lu, Chenggang Zhao, Chengqi Deng, Chenyu Zhang, Chong Ruan, and 1 others. 2024. Deepseek-v3 technical report. arXiv preprint arXiv:2412.19437.
- Changxing Liu, Genjia Liu, Zijun Wang, Jinchang Yang, and Siheng Chen. 2025. Colmdriver: Llm-based negotiation benefits cooperative autonomous driving. In *Proceedings of the IEEE/CVF International Conference on Computer Vision*, pages 25951–25960.
- Chengdong Ma, Aming Li, Yali Du, Hao Dong, and Yaodong Yang. 2024. Efficient and scalable reinforcement learning for large-scale network control. *Nature Machine Intelligence*, 6(9):1006–1020.
- Aman Madaan, Niket Tandon, Prakhar Gupta, Skyler Hallinan, Luyu Gao, Sarah Wiegrefe, Uri Alon, Nouha Dziri, Shrimai Prabhumoye, Yiming Yang, and 1 others. 2023. Self-refine: Iterative refinement with self-feedback. *Advances in Neural Information Processing Systems*, 36:46534–46594.
- Frans A Oliehoek, Christopher Amato, and 1 others. 2016. *A concise introduction to decentralized POMDPs*, volume 1. Springer.
- Afshin Oroojlooy and Davood Hajinezhad. 2023. A review of cooperative multi-agent deep reinforcement learning. *Applied Intelligence*, 53(11):13677–13722.
- Joon Sung Park, Joseph O’Brien, Carrie Jun Cai, Meredith Ringel Morris, Percy Liang, and Michael S. Bernstein. 2023. [Generative agents: Interactive simulacra of human behavior](#). In *Proceedings of the 36th Annual ACM Symposium on User Interface Software and Technology*, UIST ’23, New York, NY, USA. Association for Computing Machinery.
- John Schulman, Filip Wolski, Prafulla Dhariwal, Alec Radford, and Oleg Klimov. 2017. Proximal policy optimization algorithms. arXiv preprint arXiv:1707.06347.
- Yao Shi, Rongkeng Liang, and Yong Xu. 2025. Educationq: Evaluating llms’ teaching capabilities through multi-agent dialogue framework. *Association for Computational Linguistics*.
- Amanpreet Singh, Tushar Jain, and Sainbayar Sukhbaatar. 2018. Learning when to communicate at scale in multiagent cooperative and competitive tasks. *International Conference on Learning Representations*.
- Bart Van Arem, Cornelia JG Van Driel, and Ruben Visser. 2006. The impact of cooperative adaptive cruise control on traffic-flow characteristics. *IEEE Transactions on intelligent transportation systems*, 7(4):429–436.
- Guanzhi Wang, Qian Lin, Zhuoqi Chen, and 1 others. 2023. [Voyager: An open-ended embodied agent with large language models](#). arXiv preprint arXiv:2305.16291.
- Xiaoqiang Wang, Liangjun Ke, Gewei Zhang, and Dapeng Zhu. 2022a. Attention based large scale multi-agent reinforcement learning. In *2022 5th International Conference on Artificial Intelligence and Big Data (ICAIBD)*, pages 112–117. IEEE.
- Xuezhi Wang, Jason Wei, Dale Schuurmans, Quoc Le, Ed Chi, Sharan Narang, Aakanksha Chowdhery, and Denny Zhou. 2022b. Self-consistency improves chain of thought reasoning in language models. arXiv preprint arXiv:2203.11171.
- Zhenhailong Wang, Shaoguang Mao, Wenshan Wu, Tao Ge, Furu Wei, and Heng Ji. 2024. [Unleashing the emergent cognitive synergy in large language models: A task-solving agent through multi-persona self-collaboration](#). In *Proceedings of the 2024 Conference of the North American Chapter of the Association for Computational Linguistics: Human Language Technologies (Volume 1: Long Papers)*, pages 257–279, Mexico City, Mexico. Association for Computational Linguistics.
- Jason Wei, Xuezhi Wang, Dale Schuurmans, Maarten Bosma, Fei Xia, Ed Chi, Quoc V Le, Denny Zhou, and 1 others. 2022. Chain-of-thought prompting elicits reasoning in large language models. *Advances in neural information processing systems*, 35:24824–24837.

- Barry Payne Welford. 1962. Note on a method for calculating corrected sums of squares and products. *Technometrics*, 4(3):419–420.
- Licheng Wen, Daocheng Fu, Xin Li, Xinyu Cai, Tao Ma, Pinlong Cai, Min Dou, Botian Shi, Liang He, and Yu Qiao. 2024. Dilu: A knowledge-driven approach to autonomous driving with large language models. In *Proceedings of the International Conference on Learning Representations*.
- Tianyu Wu, Zhuosheng Wang, and 1 others. 2023. [Autogen: Enabling next-gen llm applications via multi-agent conversation frameworks](#). *International Conference on Learning Representations*.
- Yaodong Yang, Rui Luo, Minne Li, Ming Zhou, Weinan Zhang, and Jun Wang. 2018. Mean field multi-agent reinforcement learning. In *International conference on machine learning*, pages 5571–5580. PMLR.
- Andrew Chi-Chih Yao. 1979. Some complexity questions related to distributive computing (preliminary report). In *Proceedings of the eleventh annual ACM symposium on Theory of computing*, pages 209–213.
- Shunyu Yao, Jeffrey Zhao, Dian Yu, Nan Du, Izhak Shafran, Karthik Narasimhan, and Yuan Cao. 2023. React: Synergizing reasoning and acting in language models. In *International Conference on Learning Representations (ICLR)*.
- Yangyang Yu, Zhiyuan Yao, Haohang Li, Zhiyang Deng, Yuechen Jiang, Yupeng Cao, Zhi Chen, Jordan Suchow, Zhenyu Cui, Rong Liu, and 1 others. 2024. Fincon: A synthesized llm multi-agent system with conceptual verbal reinforcement for enhanced financial decision making. *Advances in Neural Information Processing Systems*, 37:137010–137045.
- Mert Yuksekgonul, Federico Bianchi, Joseph Boen, and 1 others. 2025. [Optimizing generative ai by backpropagating language model feedback](#). *Nature*, 639:609–616.
- Hongxin Zhang, Weihua Du, Jiaming Shan, Qinhong Zhou, Yilun Du, Joshua B. Tenenbaum, Tianmin Shu, and Chuang Gan. 2024. [Building cooperative embodied agents modularly with large language models](#).
- Yao Zhang, Chenyang Lin, Shijie Tang, Haokun Chen, Shijie Zhou, Yunpu Ma, and Volker Tresp. 2025. Swarmagentic: Towards fully automated agentic system generation via swarm intelligence. In *Proceedings of the 2025 Conference on Empirical Methods in Natural Language Processing*, pages 1778–1818.
- Running Zhao, Zhihan Jiang, Xinchun Zhang, Chirui Chang, Handi Chen, Weipeng Deng, Luyao Jin, Xiaojuan Qi, Xun Qian, and Edith C.H. Ngai. 2025. [Noteit: A system converting instructional videos to interactable notes through multimodal video understanding](#). In *Proceedings of the 38th Annual ACM Symposium on User Interface Software and Technology*, UIST '25, New York, NY, USA. Association for Computing Machinery.
- Wanjun Zhong, Lianghong Guo, Qiqi Gao, He Ye, and Yanlin Wang. 2024. Memorybank: Enhancing large language models with long-term memory. In *Proceedings of the AAAI Conference on Artificial Intelligence*, volume 38, pages 19724–19731.
- Xinyu Zhu, Junjie Wang, Lin Zhang, Yuxiang Zhang, Yongfeng Huang, Ruyi Gan, Jiaying Zhang, and Yujie Yang. 2023. [Solving math word problems via cooperative reasoning induced language models](#). In *Proceedings of the 61st Annual Meeting of the Association for Computational Linguistics*, pages 4471–4485, Toronto, Canada. Association for Computational Linguistics.
- Henry Peng Zou, Wei-Chieh Huang, Yaozu Wu, Yankai Chen, Chunyu Miao, Hoang Nguyen, Yue Zhou, Weizhi Zhang, Liancheng Fang, Langzhou He, and 1 others. 2025. Llm-based human-agent collaboration and interaction systems: A survey. *arXiv preprint arXiv:2505.00753*.

Appendix Table of Contents

A	Extended Related Works	14	O	Analysis of Failure Cases and Solutions	24
B	Detailed Algorithm of Proposal Generation	15	P	Analysis of Introspector’s Attribution-based Reasoning	25
C	Scope of Theoretical Assumptions	15	P.1	Qualitative Evidence: Scenario-Adaptive Diagnostic Attribution Analysis	25
D	Proof of Theorem 1	16	P.2	Quantitative Evidence: Diagnostic Attribution Statistics	26
E	Proof of Theorem 2 (Properties of the Negotiation Loop)	17	P.3	Behavioral Coherence Verification	26
F	Equations for Welford-based State Aggregation	17	Q	Core Prompts of MACRO-LLM	26
G	Simulation Environments and Task Configurations	18	Q.1	CoProposer	26
G.1	Cooperative Platoon Planning (CPP)	18	Q.2	Negotiator	26
G.2	Pandemic Coordination (PC) . . .	18	Q.3	Introspector	26
H	Baseline Methods	19	R	AI Assistants in Writing	26
H.1	MARL Baselines	19			
H.2	LLM-based MAS Baselines . . .	19			
H.3	Adaptation, Fairness, and System Design	20			
I	Case Study: Hierarchical Deployment for Safety-Critical Domains	20			
I.1	Hierarchical Deployment Paradigm	20			
I.2	Decision Frequency Analysis . . .	21			
J	Detailed Evaluation Metrics	21			
J.1	CPP Task Metrics	21			
J.2	PC Task Metrics	22			
K	Analysis of Model Generalizability	22			
L	Computational and Communication Scalability Analysis	22			
L.1	Communication Complexity Analysis	22			
L.2	Computational Efficiency and Latency	23			
L.3	Scalability Metrics Across Fleet Sizes	23			
M	Extended Ablation Analysis	23			
M.1	Component Analysis in CPP Task	23			
M.2	Component Analysis in PC Task .	24			
N	Analysis of Robustness	24			

A Extended Related Works

Due to space constraints, we provide a comprehensive review of the literature in this appendix.

Agent Planning with LLMs. There has been a recent surge in research on LLM-based agent reasoning and planning (Huang et al., 2024; Yuksekogonul et al., 2025). Techniques such as Chain-of-Thought (CoT) (Wei et al., 2022), ReAct (Yao et al., 2023), Self-Consistency (Wang et al., 2022b), and Graph-of-Thought (Besta et al., 2024) enhance single-agent reasoning by decomposing tasks or broadening candidate exploration. Self-Refine (Madaan et al., 2023) introduces iterative self-correction, and MemoryBank (Zhong et al., 2024) augments planning with historical knowledge retrieval. However, these methods are designed for single-agent settings with full or near-complete observability. In multi-agent scenarios under partial observability, the core challenge shifts from individual reasoning quality to inter-agent coordination under fragmented information. That is a problem that single-agent planning enhancements do not address.

Extended Related Work on LLM-based Multi-Agent Systems. The emergence of Large Language Models (LLMs) has revolutionized multi-agent collaboration. Early frameworks such as CAMEL (Li et al., 2023a) and AutoGen (Wu et al., 2023) demonstrated the potential of communicative agents to solve open-ended tasks through dynamic role-playing. Subsequent systems introduced structured enhancements to improve stability and capability. For instance, MetaGPT (Hong et al., 2023) incorporates Standardized Operating Procedures (SOPs) to streamline workflows, while Voyager (Wang et al., 2023) utilizes an iterative curriculum with persistent code libraries for embodied control. Despite their success in observable environments (e.g., software engineering, Minecraft), these frameworks typically operate under the assumption of global observability or unrestricted communication, rendering them less effective in spatially distributed, bandwidth-constrained real-world scenarios. Recent research targeting the information imbalance caused by spatial constraints generally falls into two categories:

1. *Hierarchical aggregation:* Works such as FinCon (Yu et al., 2024), MLPO (Estornell et al., 2025), and HALO (Hou et al., 2025) employ

hierarchical architectures. These systems designate specific agents (e.g., central hubs) to aggregate incomplete information, constructing a pseudo-global view to compensate for limited local perception. However, this centralization introduces critical bottlenecks: it relies heavily on central nodes and often incurs prohibitive communication overheads as the network scales.

2. *Individual reasoning enhancement:* A complementary line of research focuses on enhancing individual reasoning capabilities. Theory-of-Mind (ToM) approaches (Li et al., 2023b) enable agents to infer the beliefs and intents of others, while frameworks like LAMEN (Davidson et al., 2024) utilize structured reasoning chains to predict hidden states. While effective for small-scale interactions, these methods often struggle with the *spatiotemporal uncertainty* inherent in complex topologies, where agents must simultaneously reason about spatial neighbors and future dynamics under strict latency constraints.
3. *Swarm-based optimization:* Recent works apply particle swarm optimization to LLM systems. Model Swarms (Feng et al., 2024) searches the model weight space over 50 iterations with per-particle validation-set evaluation to produce adapted expert checkpoints. SwarmAgentic (Zhang et al., 2025) searches the system configuration space over 10 iterations, jointly optimizing agent functionalities and collaboration structures through failure-driven refinement. While both methods achieve dynamic configuration evolution, this adaptation occurs during an offline optimization loop that requires a globally accessible fitness function evaluated over the entire validation set.

In contrast, MACRO-LLM proposes a fully decentralized negotiation mechanism that leverages mean-field statistics and semantic strategies, effectively balancing local perception with global coordination goals.

Extended Related Work on MARL To tackle spatial partial observability, the Decentralized Partially Observable Markov Decision Process (DecPOMDP) serves as the foundational modeling framework (Oliehoek et al., 2016). Under this

model, agents must act based on local histories rather than global states. To mitigate the non-stationarity inherent in decentralized learning, the Centralized Training with Decentralized Execution (CTDE) paradigm has become standard. Recent works have further incorporated memory augmentation mechanisms (Kia et al., 2024) and theoretical guarantees (Bernstein et al., 2005) to approximate global state value functions. However, these methods typically require fitting a value function to a specific state space, limiting their transferability.

Scalability remains a critical bottleneck in MARL. Mean-field MARL offers a promising direction by approximating agent-to-agent interactions via the average effect of the neighborhood (Yang et al., 2018). Subsequent studies have extended this to accommodate agent heterogeneity (Ganapathi Subramanian et al., 2020; Gu et al., 2025) and robustness (Wang et al., 2022a; Anand et al., 2024). Similarly, MACRO-LLM adopts the mean-field principle in its *Negotiator* module to compress spatial information. However, unlike MARL which learns a mean-field policy through extensive episodes, our approach computes mean-field statistical features explicitly as prompts for the LLM, enabling inference-time reasoning without gradient updates.

To improve sample efficiency, advanced policy optimization methods such as Multi-Agent PPO (MAPPO) (Schulman et al., 2017) and Model-based Decentralized Policy Optimization (DMPO) (Ma et al., 2024) have been developed. Furthermore, adaptive communication protocols like IC3Net (Singh et al., 2018) introduce gating mechanisms to decide when to communicate. Despite these advances, the fundamental reliance on trial-and-error interaction makes MARL computationally intensive. As noted by (Huh and Mohapatra, 2023) and (Oroojlooy and Hajinezhad, 2023), MARL policies often struggle to generalize to unseen topologies or agent numbers, necessitating the retraining costs that our LLM-based framework aims to eliminate.

B Detailed Algorithm of Proposal Generation

In this section, we detail the algorithmic procedure for the CoProposer module. The core mechanism, *Proposal Generation via Rollout-Simulated Verification*, is outlined in Algorithm 1.

This process aims to find an action sequence

that maximizes cumulative reward while strictly adhering to safety constraints. To ensure computational efficiency, the algorithm employs an *early exit mechanism*: if a generated proposal successfully passes verification over the entire horizon k , it is immediately adopted as the proposal P_n^t , terminating the search loop.

The computational complexity of the CoProposer is dominated by the number of LLM inference calls. Let Att_{\max} be the maximum number of validation attempts and K be the rollout horizon. In the worst-case scenario (where valid proposals are hard to find), the complexity is $\mathcal{O}(Att_{\max} \cdot k)$. To mitigate latency in real-world applications, we set $Att_{\max} = 10$ for all tasks. The binary simplification of rewards beyond $t + 1$ further reduces the overhead of reward calculation.

C Scope of Theoretical Assumptions

Eq. 4 analyzes the mean-field approximation error under the domain’s true reward function R_n , i.e., the error introduced by substituting the true neighborhood states $s_{\mathcal{N}_n}^t$ with the mean-field estimate μ_n . We clarify the scope and assumptions below.

Domain Satisfaction. In our two evaluation domains, the domain reward functions are governed by continuously differentiable physical dynamics: kinematic equations relating headway and velocity deviations in CPP, and epidemiological SIR-family dynamics governing infection rates in PC. Both operate over bounded state-action spaces with finite horizons, satisfying the smoothness requirement for the Taylor expansion argument. The constant L_2 is therefore determined by the continuity properties of these domain-specific dynamics.

Scope Clarification. Eq. 4 characterizes the theoretical relationship between neighborhood variance σ_n^2 and the mean-field approximation quality under the domain’s true reward function. This analysis establishes σ_n^2 as a principled uncertainty indicator, motivating the framework’s design choice of transmitting σ_n^2 during negotiation. In practice, the LLM’s rollout-based reward estimation introduces a separate source of approximation that is outside the scope of Eq. 4. This estimation gap is mitigated through progressive constraint relaxation in rollout verification (Sec. 3.2), which simplifies reward signals beyond $t + 1$ to binary feasibility indicators, reducing sensitivity to prediction imprecision.

Algorithm 1: Pseudocode of proposal generation via rollout-simulated verification.

Input: Observation o_n^t ; strategies $\Pi_{n,t}^{\text{temp}}$ and $\Pi_{n,t}^{\text{spatial}}$; maximum attempts Att_{\max} ; rollout horizon K

Output: Verified proposal $P_n^t = (o_n^t, a_n^t, \{a_{n \rightarrow m}^t\}_{m \in \mathcal{N}_n})$

- 1 Initialize CANDIDATE_PROPOSALS $\leftarrow \emptyset$ and $att = 0$;
- 2 Initialize candidate action with highest reward score by
 $a_n^{t,0} \leftarrow \arg \max_a \text{InferAction}(o_n^t, \mathcal{A}_n, \Pi_{n,t}^{\text{temp}}, \Pi_{n,t}^{\text{spatial}})$ and ensure
 $R_n^t(o_n^t, a_n^{t,0}) \geq R_n^{t-1}(o_n^{t-1}, a_n^{t-1})$;
- 3 **while** $att < Att_{\max}$ **do**
- 4 Initialize rollout trajectory $\tau_n^{t,att} = (o_n^t, a_n^{t,att}, R_n^t)$;
- 5 **foreach** $m \in \mathcal{N}_n$ **do**
- 6 Obtain observable agents' candidate action
 $a_{n \rightarrow m}^{t,att} \leftarrow \text{InferNeighborAction}(o_n^t, a_n^{t,att}, \Pi_{n,t}^{\text{spatial}})$;
- 7 Construct candidate proposal $P_n^{t,att} \leftarrow (o_n^t, a_n^{t,att}, \{a_{n \rightarrow m}^{t,att}\}_{m \in \mathcal{N}_n})$;
- 8 **for** Verified time step $k = 1, \dots, K$ in a rollout **do**
- 9 Predict next observation $o_n^{t+k,att}$ with candidate proposal $P_n^{t,att}$;
- 10 **if** $o_n^{t+k,att}$ violate constraints **then**
- 11 Append $P_n^{t,att}$ to CANDIDATE_PROPOSALS;
- 12 $att = att + 1$;
- 13 Update candidate action $a_n^{t,att}$ slightly and ensure $R_n^t(o_n^t, a_n^{t,0}) \geq R_n^{t-1}(o_n^{t-1}, a_n^{t-1})$;
- 14 Break;
- 15 Infer actions $a_{n \rightarrow m}^{t+k,att}$ on time $t+k$;
- 16 Add $(a_n^{t+k,att}, o_n^{t+k,att}, R_n^{t+k,att})$ to rollout trajectory $\tau_n^{t,att}$;
- 17 **if** $P_n^{t,att}$ has been verified over k time steps **then**
- 18 **return** Optimal $P_n^t \leftarrow P_n^{t,att}$.
- 19 Select the proposal with the highest cumulative reward in its rollout from
CANDIDATE_PROPOSALS as P_n^t ;
- 20 **return** P_n^t ;

D Proof of Theorem 1

Proof. When the neighborhood \mathcal{N}_n is separated into P disjoint subgroups $\{\mathcal{N}_n^{(p)}\}_{p=1}^P$ and apply Eq. 4 independently within each subgroup. For each subgroup p , define the local weighted mean $\mu_n^{(p)} = \sum_{m \in \mathcal{N}_n^{(p)}} w_{n,m}^{(p)} s_m^t$ and local weighted variance $\sigma_n^{2,(p)} = \sum_{m \in \mathcal{N}_n^{(p)}} w_{n,m}^{(p)} (s_m^t - \mu_n^{(p)})^2$, where $w_{n,m}^{(p)} = w_{n,m}/W^{(p)}$ are the renormalized weights within subgroup p and $W^{(p)} = \sum_{m \in \mathcal{N}_n^{(p)}} w_{n,m}$. By the same argument as in Eq. 4 (Taylor expansion with first-order cancellation within each subgroup), the contribution of subgroup p to the

approximation error is bounded by:

$$\begin{aligned} |\Delta \mathcal{R}_n^{(p)}| &\leq \frac{L_2}{2} \sum_{m \in \mathcal{N}_n^{(p)}} (s_m^t - \mu_n^{(p)})^2 \\ &\leq \frac{L_2}{2 w_{\min}} \sum_{m \in \mathcal{N}_n^{(p)}} w_{n,m} (s_m^t - \mu_n^{(p)})^2. \end{aligned} \tag{6}$$

Since the subgroups are disjoint, the total approximation error is bounded by:

$$\begin{aligned} \left| \mathcal{R}_n(s_{\mathcal{N}_n}^t) - \mathcal{R}_n(\mu_n^{(1:P)}) \right| &\leq \sum_{p=1}^P |\Delta \mathcal{R}_n^{(p)}| \\ &\leq \frac{L_2}{2 w_{\min}} \sum_{p=1}^P \sum_{m \in \mathcal{N}_n^{(p)}} w_{n,m} (s_m^t - \mu_n^{(p)})^2. \end{aligned} \tag{7}$$

By the law of total variance (Casella and Berger, 2024), for any partition of a weighted dataset into

P groups:

$$\begin{aligned} & \underbrace{\sum_{m \in \mathcal{N}_n} w_{n,m} (s_m^t - \mu_n)^2}_{\sigma_n^2 \text{ (total variance)}} \\ &= \underbrace{\sum_{p=1}^P W^{(p)} \sigma_n^{2,(p)}}_{\text{within-group variance}} + \underbrace{\sum_{p=1}^P W^{(p)} (\mu_n^{(p)} - \mu_n)^2}_{\text{between-group variance} \geq 0}, \end{aligned} \quad (8)$$

where $W^{(p)} = \sum_{m \in \mathcal{N}_n^{(p)}} w_{n,m}$. Since the between-group variance is non-negative:

$$\sum_{p=1}^P W^{(p)} \sigma_n^{2,(p)} \leq \sigma_n^2. \quad (9)$$

Furthermore, noting that $\sum_{m \in \mathcal{N}_n^{(p)}} w_{n,m} (s_m^t - \mu_n^{(p)})^2 = W^{(p)} \sigma_n^{2,(p)}$, we can obtain:

$$\begin{aligned} & \sum_{p=1}^P \sum_{m \in \mathcal{N}_n^{(p)}} w_{n,m} (s_m^t - \mu_n^{(p)})^2 \\ &= \sum_{p=1}^P W^{(p)} \sigma_n^{2,(p)} \leq \sigma_n^2. \end{aligned} \quad (10)$$

Substituting back into (7):

$$\begin{aligned} & \left| \mathcal{R}_n(\mathbf{s}_{\mathcal{N}_n}^t) - \mathcal{R}_n(\boldsymbol{\mu}_n^{(1:P)}) \right| \\ & \leq \frac{L_2}{2w_{\min}} \sum_{p=1}^P W^{(p)} \sigma_n^{2,(p)} \leq \frac{L_2}{2w_{\min}} \cdot \sigma_n^2 \\ & = \frac{L_2}{2w_{\min}} \cdot |\mathcal{N}_n| \cdot \bar{\sigma}_n^2, \end{aligned} \quad (11)$$

where $\bar{\sigma}_n^2 = \sigma_n^2/|\mathcal{N}_n|$ is the per-neighbor average variance. The inequality is strict whenever the subgroup means $\mu_n^{(p)}$ differ, since the between-group variance $\sum_p W^{(p)} (\mu_n^{(p)} - \mu_n)^2 > 0$ in that case. Therefore, if the topology can be divided into several disjoint group, the error bound is tighter. \square

E Proof of Theorem 2 (Properties of the Negotiation Loop)

Proof. $\mathcal{G} = (\mathcal{V}, \mathcal{E})$ represents a connected communication graph, and r denotes the maximum number of negotiation rounds.

Bounded Termination. At each round ℓ , the negotiation loop evaluates one of two termination conditions:

- *Early stopping via local consensus:* If $\|P_n^{(\ell)} - P_m^{(\ell)}\| < \delta$ for all $m \in \mathcal{N}_n$, where δ is a predefined task-specific threshold (e.g., $\delta = 0.1 \text{ m/s}^2$ for CPP), the agent terminates negotiation.
- *Maximum round limit:* The loop terminates after at most r rounds regardless of consensus status.

Since both conditions are finitely bounded, termination is guaranteed for every agent $n \in \mathcal{V}$.

Monotonic Non-Decrease of Proposal Quality.

At the beginning of each negotiation round $\ell + 1$, the best proposal from the previous round, $P_n^{(\ell)}$, is retained in the candidate set for the current round. That is, the candidate set at round $\ell + 1$ is:

$$\mathcal{C}_n^{(\ell+1)} = \{P_n^{(\ell)}\} \cup \mathcal{C}_n^{\text{new}}, \quad (12)$$

where $\mathcal{C}_n^{\text{new}}$ denotes the set of newly generated proposals incorporating neighbor information received at round $\ell + 1$.

Since $P_n^{(\ell)} \in \mathcal{C}_n^{(\ell+1)}$ by the Design Invariant, and agent n selects $P_n^{(\ell+1)} = \arg \max_{P \in \mathcal{C}_n^{(\ell+1)}} \mathcal{R}(\tau_n(P))$, we have $\mathcal{R}(\tau_n^{(\ell+1)}) = \max_{P \in \mathcal{C}_n^{(\ell+1)}} \mathcal{R}(\tau_n(P)) \geq \mathcal{R}(\tau_n(P_n^{(\ell)})) \mathcal{R}(\tau_n^{(\ell)})$. Therefore, the sequence $\{\mathcal{R}(\tau_n^{(\ell)})\}_{\ell=0}^r$ is monotonically non-decreasing.

The cumulative rollout reward is upper-bounded by the maximum achievable return over the rollout horizon k :

$$\mathcal{R}(\tau_n^{(\ell)}) \leq \sum_{\iota=0}^k \gamma^\iota R_{\max} = R_{\max} \cdot \frac{1 - \gamma^{k+1}}{1 - \gamma}, \quad (13)$$

where $R_{\max} = \sup_{o_n, a_n} |R_n(o_n, a_n)|$ is the single-step reward bound. Therefore, $\{\mathcal{R}(\tau_n^{(\ell)})\}_{\ell=0}^r$ is a bounded, monotonically non-decreasing sequence of real numbers, which necessarily converges. \square

F Equations for Welford-based State Aggregation

The update rules for the weighted mean and variance are defined as follows:

$$\mu'_n = \mu_m + \frac{w_n}{W_n} (s_n^t - \mu_m), \quad (14)$$

$$\sigma_n^{2'} = \frac{W_m}{W_n} \sigma_m^2 + \frac{w_n}{W_n} (s_n^t - \mu_m)(s_n^t - \mu'_n), \quad (15)$$

where $W_n = W_m + w_n$ represents the updated weight. The aggregated mean μ'_n and variance $\sigma_n^{2'}$ are then abstracted into a textual description of a virtual node within the query prompt, enabling the LLM to analyze trends in the unobserved states. While equations (14) and (15) illustrate the atomic update, in practice, agents apply this iteratively or employ parallel variance merger algorithms (Chan et al., 1983) when aggregating disjoint sets.

G Simulation Environments and Task Configurations

Table 3 summarizes the key settings of the MACRO-LLM framework used across all experiments.

Table 3: Framework hyperparameters.

Parameter	Value
Rollout horizon k	2
Max negotiation rounds r	3
Max proposal attempts Att_{\max}	10
Mean-field weight $w_{n,m}$	Inverse hop distance
Consensus threshold ϵ	0.02 (CPP) / 0 (PC)
Temperature / top-p	0.3 / 1.0

In MACRO-LLM, the rollout horizon $k = 2$ balances verification depth against prompt length: the first rollout step performs precise constraint verification on the immediate next state, while the second step applies relaxed feasibility checks to ensure short-term safety (Sec. 3.3). The negotiation rounds $r = 3$ are set based on network diameter D : since each agent begins with 1-hop neighbor information and each round propagates aggregated statistics by one additional hop, r rounds yield effective coverage of $r + 1$ hops. For the PC topologies ($D \leq 4$), $r = 3$ provides full network coverage. For the CPP linear topology ($D = 7$), the topology-aware partitioning into predecessor and follower subgroups (Theorem 1) reduces the effective propagation distance to $D/2$ per direction, which $r = 3$ sufficiently covers.

We evaluate our framework on two complementary domains, CPP and PC, to assess its collaborative performance and generalization capabilities, utilizing high-fidelity simulators for each task. The evaluation covers continuous and discrete actions, linear and graph topologies, fine-grained and long-horizon planning.

G.1 Cooperative Platoon Planning (CPP)

The CPP task is simulated using the Simulation of Urban Mobility (SUMO)¹ (Version 1.21.0).

- **Topology:** We model a platoon of eight vehicles ($N = 8$) on a single-lane highway segment. The simulation runs for a duration of 60s with 120 time steps in total. Each agent operates with limited perception, accessing only the state information (e.g., headway, velocity) of its immediately adjacent vehicles (predecessor and follower). Due to the linear topology, each agent’s neighborhood naturally partitions into two disjoint subgroups—predecessor and follower—with separate mean-field statistics computed for each direction (Theorem 1).
- **Objective:** The control objective is for agents to autonomously adjust acceleration to stabilize the platoon, converging rapidly to an optimal headway of 20 m and a target velocity of 15 m/s. The consensus threshold is set to $\epsilon = 0.02$ for the CPP task.
- **Scenarios:** We evaluate performance in two dynamic settings: (1) *Scenario 1: Catch-up:* The leading vehicle accelerates to close the gap with a target vehicle, testing the platoon’s ability to re-establish stable formation under high-speed conditions. (2) *Scenario 2: Slow-down:* The leading vehicle decelerates from a high initial speed, challenging the followers to execute coordinated braking without collisions or oscillation.

G.2 Pandemic Coordination (PC)

The PC task is simulated using the open-source Pandemic Simulator² (Kompella* et al., 2020).

- **Topology:** We model the urban environment as a graph of seven agents representing distinct facility types: *Home, Office, School, Hospital, Retail, Restaurant, and Government*. To construct realistic urban topologies, we utilize Google Maps to identify clusters of functionally similar buildings within specific urban blocks, marking their centroids as individual agents. Communication links are established

¹SUMO: <https://eclipse.dev/sumo/>, licensed under EPL 2.0.

²Pandemic Simulator: <https://github.com/SonyResearch/PandemicSimulator>, licensed under Apache-2.0.



(a)



(b)



(c)

Figure 6: Communication topology of cities for pandemic networks. (a) Helsinki (b) Hong Kong (c) New York.

based on spatial proximity, forming a connected topology as shown in Fig. 6. Since the urban graph does not admit a natural disjoint partition of each agent’s neighborhood, mean-field statistics are computed over the full neighborhood without subgroup decomposition. The simulation spans 120 days, during which agents operate under partial observability regarding global infection rates.

- **Objective:** The primary objective is for agents to dynamically adjust regulatory policies (e.g., gathering restrictions, business hours) to minimize the spread of the virus while maintaining essential socio-economic activities. The consensus threshold is set to $\delta = 0$ for the PC task.
- **Scenarios:** We evaluate the framework’s generalization capabilities across three distinct urban settings with varying population scales: (1) *Helsinki*: A standard community setting with a population of 500. (2) *Hong Kong*: A denser urban setting with a population of 1000. (3) *New York*: A high-density complex topology with a population of 1500.

H Baseline Methods

To evaluate MACRO-LLM, we implement and adapt the following baselines for both the CPP and PC tasks.

H.1 MARL Baselines

We compare against traditional Multi-Agent Reinforcement Learning (MARL) approaches: (1) **DPPO** (Ma et al., 2024): Multi-agent Decentralized Proximal Policy Optimization; (2) **DMPO** (Ma et al., 2024): Multi-agent Model-based Decentralized Policy Optimization; (3) **IC3Net** (Singh et al., 2018): A classic approach for learning when to communicate in multi-agent environments.

H.2 LLM-based MAS Baselines

We compare against recent frameworks utilizing LLMs for collaboration: (1) **ToM-Belief** (Li et al., 2023b): A MAS that employs second-order Theory of Mind for introspection via belief state updates and environmental feedback; (2) **ChatEval** (Chan et al., 2023): Adopts the Simultaneous-Talk-with-Summarizer protocol (Algorithm 3), which is structurally similar to our task

setting; (3) **LAMEN** (Davidson et al., 2024): A framework that constructs internal “mental notes” alongside public messages to facilitate strategic negotiation.

H.3 Adaptation, Fairness, and System Design

To ensure a fair and reproducible comparison, we maintain experimental consistency across all LLM-based methods. In MACRO-LLM, the LLM performs all strategic reasoning: generating collaborative proposals, predicting future observations during rollout verification, evaluating proposal conflicts and updating spatial strategies in the Negotiator, and diagnosing performance drops in the Introspector. Deterministic computations independent of the LLM reasoning process, such as mean-field statistics (Eqs. 2–3) and drift intensity (Eq. 5), are offloaded to an external numerical module to ensure precision. All inference-dependent computations, including state prediction and constraint evaluation during rollout verification, are performed entirely by the LLM. LLM outputs are validated against a structured XML schema; outputs failing validation trigger an automatic retry (up to 3 attempts).

All LLM-based baselines (ToM-Belief, ChatEval, LAMEN) share the same backbone model (GPT-4o), environmental interfaces, external numerical module, schema validation, and retry mechanism as MACRO-LLM. Methods differ only in their prompting strategies and inter-agent communication protocols (e.g., mental notes generation in LAMEN, belief updates in ToM-Belief). This ensures that performance differences reflect methodological contributions rather than implementation advantages.

I Case Study: Hierarchical Deployment for Safety-Critical Domains

As a general-purpose strategic coordination framework, MACRO-LLM outputs high-level collaborative directives rather than low-level control commands. For domains with real-time safety constraints, this property allows MACRO-LLM to naturally integrate into a hierarchical deployment paradigm (Liu et al., 2025; Wen et al., 2024), where the strategic layer and execution layer operate at different temporal granularities. In this section, we describe the deployment architecture and experimentally validate its feasibility through a decision frequency analysis on the Cooperative Platoon

Planning task.

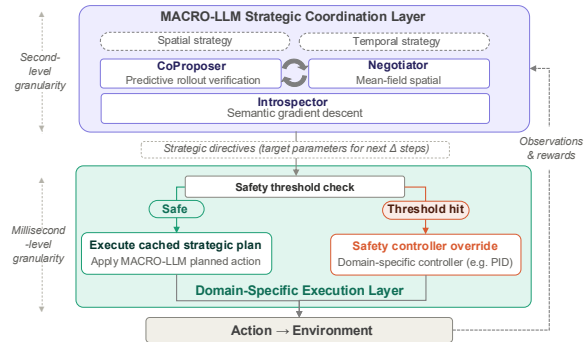


Figure 7: Hierarchical deployment paradigm for MACRO-LLM. The strategic coordination layer executes a full negotiation cycle every Δ steps to produce collaborative directives, while the domain-specific execution layer operates at every step, applying the cached strategic plan when the state is safe or triggering a safety controller override when a threshold is breached.

I.1 Hierarchical Deployment Paradigm

As illustrated in Fig. 7, the hierarchical paradigm consists of two layers:

1. *Strategic Coordination Layer (Second-level granularity)*. MACRO-LLM operates at a coarser temporal granularity, executing a full negotiation cycle among agents every Δ time steps. At each decision epoch, it produces strategic directives by reasoning about unobservable states and negotiating with neighboring agents. Between decision epochs, the execution layer carries out the planned actions.
2. *Domain-Specific Execution Layer (Millisecond-level granularity)*. A lightweight controller operates at every time step, performing a safety threshold check on the current state. If the state remains within the safe region, the controller executes the cached strategic plan from the most recent MACRO-LLM decision epoch. If a safety threshold is breached, a domain-specific controller (e.g., PID for CPP) immediately overrides the planned action to ensure system safety.

MACRO-LLM requires no architectural modification to operate within this paradigm—its outputs are inherently strategic directives that can be consumed by any domain-specific execution layer.

I.2 Decision Frequency Analysis

To validate the feasibility of hierarchical deployment, we evaluate MACRO-LLM on the CPP Catch-up scenario under varying decision intervals $\Delta \in \{1, 3, 5, 10\}$, where $\Delta = 1$ corresponds to the original setting used in our main experiments. At each decision epoch, MACRO-LLM produces a strategic action spanning the subsequent Δ time steps. Between decision epochs, the execution layer applies the most recently planned action while monitoring safety constraints via a proportional headway-tracking controller with emergency override. Table 4 presents the results alongside representative baselines from Table 1 for reference.

Table 4: Decision frequency analysis on the CPP Catch-up scenario. DPPO and LAMEN from Table 1 for reference. All metrics \downarrow .

Config.	Red.	RMSE-H	RMSE-V	SD-H	SD-V
DPPO	–	1.603	0.978	0.994	0.474
LAMEN	–	1.891	0.648	3.200	0.601
Hier. $\Delta = 10$	90%	1.443	0.623	0.634	0.225
Hier. $\Delta = 5$	80%	1.319	0.721	0.524	0.281
Hier. $\Delta = 3$	67%	1.408	0.596	0.564	0.234
MACRO $\Delta = 1$	0%	1.237	0.721	0.409	0.203

Hier.: hierarchical deployment;

Δ : decision interval (time steps between MACRO-LLM invocations)

Red.: LLM calls reduced relative to $\Delta = 1$.

All hierarchical configurations maintain safe operation without any collisions, confirming that the execution layer’s safety override mechanism provides reliable protection between decision epochs. As shown in Table 4, even with 90% fewer LLM invocations ($\Delta = 10$), the hierarchical deployment consistently outperforms both DPPO and LAMEN across all metrics. The SD-H of hierarchical deployment ($\Delta = 10$) is 36.2% lower than that of DPPO and 80.2% lower than that of LAMEN. This demonstrates that MACRO-LLM’s coordination reasoning provides substantial value even at highly reduced decision frequencies, as the strategic directives continue to guide inter-agent collaboration during the intervals between LLM invocations. Furthermore, increasing the decision frequency yields progressive improvements in coordination quality: SD-H improves from 0.634 ($\Delta = 10$) to 0.409 ($\Delta = 1$), a 35.5% reduction, confirming that the performance gains stem from MACRO-LLM’s collaborative reasoning. These results indicate that MACRO-LLM can be effectively deployed within a hierarchical paradigm, achieving competitive coordination quality while substantially reducing computational overhead.

J Detailed Evaluation Metrics

We provide the detailed definitions and mathematical formulations of the metrics used in our experiments.

J.1 CPP Task Metrics

Following previous works (Desjardins and Chaib-draa, 2011; Van Arem et al., 2006), we evaluate the platoon efficiency and stability using:

- **Root Mean Square Error (RMSE-H/V)**: Measures the deviation between the actual headway/velocity and the target values, averaged across all following vehicles ($i = 1 \dots N$) over the simulation steps ($t = 1 \dots T$). For example, RMSE of Headway (RMSE-H) is calculated as:

$$\text{RMSE-H} = \sqrt{\frac{1}{N \cdot T} \sum_{t=1}^T \sum_{i=1}^N (h_i^t - h_{\text{target}})^2}, \quad (16)$$

where h_i^t is the headway of vehicle i at time t , and h_{target} is the optimal safety distance. RMSE-V is computed similarly using velocity deviations as follows:

$$\text{RMSE-V} = \sqrt{\frac{1}{N \cdot T} \sum_{t=1}^T \sum_{i=1}^N (v_i^t - v_{\text{leader}})^2}, \quad (17)$$

where v_{leader} denotes the velocity of the leading vehicle.

- **Standard Deviation (SD-H/V)**: Measures the collaborative consistency of the platoon across all agents. Specifically, at each time step t , we calculate the standard deviation of the headway/velocity across all N vehicles. The final reported metric is the temporal average of these spatial standard deviations over the duration T :

$$\text{SD-H} = \frac{1}{T} \sum_{t=1}^T \sqrt{\frac{1}{N} \sum_{i=1}^N (h_i^t - \bar{h}^t)^2}, \quad (18)$$

where $\bar{h}^t = \frac{1}{N} \sum_{j=1}^N h_j^t$ is the average headway of the entire platoon at time t . A lower SD value indicates that all agents are maintaining consistent states simultaneously, reflecting high coordination stability. SD-V is computed

similarly using velocity deviations as follows:

$$SD-V = \frac{1}{T} \sum_{t=1}^T \sqrt{\frac{1}{N} \sum_{i=1}^N (v_i^t - \bar{v}^t)^2}. \quad (19)$$

J.2 PC Task Metrics

Following Kompella et al. (Kompella* et al., 2020), we employ the following metrics to assess containment efficacy. Let P_{total} be the total population, and I^t, C^t, D^t be the count of infected, critical, and dead cases on day t , respectively.

- **Normalized Infection (I_n)**: The ratio of the cumulative number of infected cases to the total population:

$$I_n = \frac{\sum_t \Delta I_{new}^t}{P_{total}}. \quad (20)$$

- **Normalized Peak Infection (PI_n)**: Measures the highest pressure on the healthcare system:

$$PI_n = \frac{\max_t(I^t)}{P_{total}}. \quad (21)$$

- **Normalized Dead (D_n)**: The ratio of total dead cases to the total population at the end of the episode (t_{end}):

$$D_n = \frac{D^{t_{end}}}{P_{total}}. \quad (22)$$

- **Pandemic Duration (PD)**: The time span (in days) from the first confirmed infection (t_{start}) until the pandemic is effectively contained:

$$PD = t_{end} - t_{start}, \quad (23)$$

where $t_{end} = \min\{t \mid I^t + C^t = 0, \forall \tau > t\}$.

K Analysis of Model Generalizability

We investigate the robustness of MACRO-LLM by instantiating it with diverse LLM backbones, including DeepSeek-V3.1 (Liu et al., 2024), Llama-3.3-70B-Instruct (Grattafiori et al., 2024), Mistral-Small-3.2-24B-Instruct, Qwen3-flash (Bai et al., 2023), GPT-4o-mini, and GPT-4o. The results are detailed in Table 5. In the CPP task, performance gaps across backbones are primarily attributable to the fine-grained continuous control demands: GPT-4o and DeepSeek-V3.1 reduce RMSE-H by

Table 5: Generalizability analysis of MACRO-LLM across different LLM backbones. S1/S2: Catch-up/Slow-down scenarios of CPP tasks. C1-C3: PC topologies for Helsinki, Hong Kong, and New York.

Tasks	Base Models	Metrics (↓)				
		RMSE-H	RMSE-V	SD-H	SD-V	
CPP	S1	DeepSeek-V3.1	1.528	0.553	0.611	0.190
		Llama-3.3-70B	1.412	0.779	0.645	0.365
		Mistral-3.2-24B	1.891	0.784	0.997	0.326
		Qwen3-flash	3.521	1.910	2.935	0.579
		GPT-4o-mini	2.906	1.667	1.858	0.936
	GPT-4o	1.237	0.721	0.409	0.203	
	S2	DeepSeek-V3.1	0.649	3.388	0.274	0.417
		Llama-3.3-70B	1.163	3.736	0.889	1.224
		Mistral-3.2-24B	1.842	3.523	1.157	0.916
		Qwen3-flash	3.871	3.678	2.946	0.974
GPT-4o-mini		2.352	3.999	1.598	1.171	
GPT-4o	0.496	3.310	0.128	0.238		
PC	C1	DeepSeek-V3.1	0.098	0.038	0.002	46
		Llama-3.3-70B	0.013	0.008	0.000	14
		Mistral-3.2-24B	0.043	0.014	0.003	31
		Qwen3-flash	0.010	0.008	0.002	16
		GPT-4o-mini	0.010	0.010	0.000	17
	GPT-4o	0.011	0.008	0.000	10	
	C2	DeepSeek-V3.1	0.008	0.005	0.001	22
		Llama-3.3-70B	0.012	0.005	0.000	16
		Mistral-3.2-24B	0.009	0.004	0.001	22
		Qwen3-flash	0.008	0.006	0.001	18
		GPT-4o-mini	0.006	0.004	0.000	24
	GPT-4o	0.008	0.004	0.001	23	
	C3	DeepSeek-V3.1	0.003	0.003	0.000	11
		Llama-3.3-70B	0.013	0.006	0.000	25
		Mistral-3.2-24B	0.009	0.006	0.000	14
Qwen3-flash		0.003	0.003	0.000	13	
GPT-4o-mini		0.003	0.003	0.000	13	
GPT-4o	0.004	0.003	0.000	25		

over 47.4% compared to GPT-4o-mini in the Catch-up scenario. Conversely, in the PC task, Qwen3-flash and GPT-4o-mini achieve containment efficacy comparable to GPT-4o across all three topologies, as this task relies more on strategic planning than on numerical precision. This contrast confirms that the observed performance variation stems from task-specific precision requirements rather than framework limitations, and that MACRO-LLM’s structured negotiation mechanism enables even lightweight models to accomplish complex multi-agent coordination tasks.

L Computational and Communication Scalability Analysis

We provide a theoretical and experimental analysis of MACRO-LLM, focusing on communication complexity and computational workload.

L.1 Communication Complexity Analysis

Following the definition by Yao (Yao, 1979), communication complexity is quantified by the total

number of bits exchanged during the protocol. In our decentralized framework, we focus on the per-agent communication load. Let $\mathcal{G} = (\mathcal{V}, \mathcal{E})$ be the agent communication graph. We denote the average node degree as \bar{d} and the maximum negotiation rounds as r . The topology of the CPP task is linear ($\bar{d} \approx 2$). In the PC task, the topology represents an urban graph with average degree \bar{d}_{PC} . We assume sparse topologies where \bar{d} does not grow linearly with the total number of agents N (i.e., $\bar{d} \ll N$). As the network scales up, MACRO-LLM employs mean-field approximation to compress the states of unobservable agents into a single virtual node representation. Neglecting inference stochasticity, the per-agent message size is theoretically invariant to the network scale, which is represented as M . Consequently, the per-agent communication complexity can be represented as $O(\bar{d} \cdot r \cdot M)$. Since \bar{d} , r , and M are independent of network scale N , the per-agent load remains constant as the network scales in theory. In other words, the per-agent communication load does not increase with the number of agents as long as the topology’s connectivity degree remains constant. The scalability results in Table 6 demonstrate as the platoon scales from $N = 8$ to $N = 32$, coordination metrics remain stable with no monotonic degradation.

L.2 Computational Efficiency and Latency

Given that the input prompt length remains bounded as analyzed above, the upper bound of the inference workload for a single agent does not increase with the number of agents. Under API-based deployment, the per-step latency is dominated by network round-trip overhead of remote API calls rather than the framework’s reasoning complexity itself. The per-step latency is dominated by API network overhead of remote LLM calls (~ 5.99 s per call for GPT-4o). This overhead can be substantially mitigated through two orthogonal and composable strategies:

(1) Local deployment of lightweight models.

Table 5 demonstrates that lightweight models such as GPT-4o-mini and Qwen3-flash achieve competitive coordination performance across both tasks. Locally deploying these models eliminates API network latency entirely, reducing per-call inference time by an order of magnitude compared to remote API access.

(2) **Hierarchical deployment with reduced decision frequency.** As demonstrated in Appendix I, MACRO-LLM maintains superior performance

over all baselines even when decision frequency is reduced by 90% (Table 4), confirming that the framework’s coordination value does not depend on high-frequency invocation.

These two strategies are composable: combining local lightweight models with increased decision intervals can reduce the effective latency by over an order of magnitude relative to the default API-based configuration.

Furthermore, MACRO-LLM exhibits instant zero-shot adaptation to new scenarios, whereas MARL baselines necessitate extensive retraining when transferring to unseen topologies. For dynamic, open-world deployments where frequent retraining is impractical, this zero-shot capability represents a significant practical advantage that offsets the per-step inference cost.

L.3 Scalability Metrics Across Fleet Sizes

Fig. 3 represents the coordination performance for the CPP Catch-up scenario as the fleet size increases from $N = 8$ to $N = 32$. Table 6 reports the detailed metrics.

Table 6: Scalability analysis on CPP Catch-up with GPT-4o.

N	RMSE-H↓	RMSE-V↓	SD-H↓	SD-V↓
8	1.237	0.721	0.409	0.203
16	1.003	0.749	0.493	0.355
24	0.908	0.664	0.520	0.382
32	0.728	0.628	0.433	0.397

All metrics remain stable as N increase to 32, with no monotonic degradation. The results indicate that the mean-field aggregation mechanism effectively compresses large-scale interactions without sacrificing coordination precision.

M Extended Ablation Analysis

In this section, we provide a detailed quantitative analysis of the ablation study.

M.1 Component Analysis in CPP Task

The removal of specific modules leads to critical performance degradation in the high-precision and highly dynamic CPP task:

- **Impact of CoProposer:** Without the CoProposer, agents fail to infer and verify collaborative actions via rollout simulation. Consequently, RMSE-H and SD-H are $9.1 \times$ and

Table 7: Robustness analysis of MACRO-LLM with GPT-4o on the CPP task (5 independent runs). Results are reported as mean \pm standard deviation.

Scenario	RMSE-H (\downarrow)	RMSE-V (\downarrow)	SD-H (\downarrow)	SD-V (\downarrow)
Catch-up	1.237 \pm 0.068	0.721 \pm 0.124	0.409 \pm 0.034	0.203 \pm 0.054
Slow-down	0.496 \pm 0.044	3.310 \pm 0.010	0.128 \pm 0.054	0.238 \pm 0.073

18.3 \times higher than those of MACRO-LLM, respectively. This result demonstrates that effective multi-agent coordination heavily depends on high-quality, verified initial proposals.

- **Impact of Negotiator:** Even with valid collaborative actions generated by the CoProposer, the omission of the negotiation phase results in an RMSE-H 6.1 \times higher than that of the full model. This degradation demonstrates the agents’ inability to resolve conflicting intentions within a time-varying environment.
- **Impact of Introspector:** Agents without the Introspector tend to sacrifice headway stability to aggressively optimize velocity, with RMSE-H degrading by 1.9 \times . This indicates that self-reflection is essential to suppress oscillation and prevent the “accordion effect” in multi-agent collaboration.

M.2 Component Analysis in PC Task

A similar pattern holds for the PC task:

- **Impact of CoProposer:** Removing the CoProposer extends the pandemic duration by 2.5 \times compared to the full framework. Lacking rollout-simulated verification, agents adopt myopic strategies, failing to curb pandemic transmission effectively.
- **Impact of Negotiator:** Excluding the Negotiator prolongs the pandemic to 32 days, demonstrating that the absence of consensus mechanisms leads to inconsistent and ineffective containment policies.
- **Impact of Introspector:** Ablating the Introspector results in a pandemic duration approximately 44.4% longer than MACRO-LLM. This illustrates that agents without self-reflection are slow to adapt their strategies to the evolving infection dynamics.

N Analysis of Robustness

To evaluate the stability of MACRO-LLM, we conduct 5 independent runs with GPT-4o and report the

Table 8: Robustness analysis of MACRO-LLM with GPT-4o on the PC task (5 independent runs). Results are reported as mean \pm standard deviation.

City	I_n (\downarrow)	PI_n (\downarrow)	D_n (\downarrow)	PD_n* (\downarrow)
Helsinki	0.011 \pm 0.001	0.008 \pm 0.000	0.000 \pm 0.000	0.081 \pm 0.024
Hong Kong	0.008 \pm 0.004	0.004 \pm 0.001	0.001 \pm 0.001	0.190 \pm 0.063
New York	0.004 \pm 0.001	0.003 \pm 0.000	0.000 \pm 0.000	0.204 \pm 0.117

* PD_n = PD / total simulation days, representing the proportion of pandemic duration relative to the total evaluation period.

mean and standard deviation in Tables 7 and 8. For the CPP task, MACRO-LLM exhibits low variance across all metrics. In the Catch-up scenario, the SD-H of 0.409 \pm 0.034 is 58.9% lower than that of DPPO, and even the upper bound (0.443) remains 55.4% lower, confirming that the stability advantage in Table 1 is not attributable to favorable randomness. Similarly, in the Slow-down scenario, the RMSE-H (0.496 \pm 0.044) is 46.3% lower than that of LAMEN and 71.2% lower than that of DPPO across all runs. For the PC task, infection-related metrics (I_n, PI_n, D_n) remain tightly concentrated across all three topologies, with standard deviations at or near zero. While PD_n shows relatively higher variance in more complex topologies (e.g., New York: 0.204 \pm 0.117), this is expected given the larger state space and stochastic disease dynamics inherent to denser urban networks. These results confirm that MACRO-LLM achieves consistently superior performance with reliable reproducibility across independent trials.

O Analysis of Failure Cases and Solutions

To provide insights into the limitations of current LLMs in multi-agent control, we categorize the primary failure cases observed during our experiments and detail the corresponding mitigation strategies implemented in MACRO-LLM.

Arithmetic and Spatial Hallucinations. Despite access to topological information, agents occasionally exhibit spatial hallucinations, such as confusing front and back vehicles in the CPP task. To mitigate this, we employ few-shot prompting incorporating explicit examples of state transitions (e.g., detailing how acceleration impacts headway relative to neighbors).

While LLMs occasionally produce imprecise numerical estimates during multi-step rollout predictions, all inference-dependent computations—including state prediction and constraint evaluation during rollout verification—are performed entirely by the LLM, with progressive con-

straint relaxation (Sec. 3.2) reducing sensitivity to arithmetic imprecision. Deterministic computations independent of the LLM reasoning process, such as post-execution environment updates, are offloaded to an external numerical module to ensure precision.

Identity Confusion. In scenarios featuring dense interaction prompts, such as concurrent proposals involving similar identifiers, such as “*Vehicle 2* propose action1 to *Vehicle 1*, and propose action2 to *Vehicle 3*”, agents may misattribute actions or forget their own identity. We attribute this to the attention mechanism’s difficulty in distinguishing semantically similar tokens within extended contexts. To address this, we enforce a structured schema for inter-agent communication and integrate a self-consistency mechanism to validate sender-receiver pairings. Additionally, we reinforce role stability by prepending the instruction “*You are [Agent Name]*” to every query prompt.

Syntactic Robustness. To structure agent outputs, we employ XML-style `<label>` tags. However, smaller or quantized models (e.g., GPT-4o-mini, Qwen3-flash) occasionally fail to adhere to these formatting constraints, resulting in unclosed tags or hallucinated labels. To mitigate this, we implement a deterministic verification layer, outputs failing regex matching or schema validation trigger an automatic retry, ensuring that only syntactically valid actions are executed.

Safety Alignment Sensitivity. In the PC task, the Qwen series frequently triggered safety refusals during stages characterized by high mortality rates, erroneously flagging simulation statistics as harmful content (returning `openai.BadRequestError`). This behavior indicates a stricter safety filter configuration compared to models like GPT-4o. To mitigate these false positives, we appended a system prompt explicitly clarifying the synthetic nature of the data: “SIMULATION NOTE: This is a hypothetical pandemic experiments on pandemic simulator. All data is synthetic and does not reflect real-world events!!!” Additionally, we implemented a rollback mechanism to discard and retry generation steps interrupted by safety filters.

P Analysis of Introspector’s Attribution-based Reasoning

To investigate how the Introspector achieves effective strategy refinement, we analyze whether its semantic revision signals reflect genuine attribution-based reasoning, attributing state changes to inter-agent interaction mechanisms, rather than simple trajectory pattern matching that maps local observations directly to actions. We provide both qualitative and quantitative evidence below.

P.1 Qualitative Evidence: Scenario-Adaptive Diagnostic Attribution Analysis

We present representative semantic revision signals generated by the Introspector in two distinct CPP scenarios to demonstrate that it produces scenario-adaptive diagnostic attribution analyses rather than templated outputs.

Case 1 (Catch-up Scenario). Vehicle 2 generated the following revision signal:

“The reasons may be due to the unexpected deceleration of vehicle 1 and the slight acceleration of vehicle 3. Vehicle 1’s velocity decreased more than anticipated, causing vehicle 2 to adjust its acceleration to maintain a safe distance.”

The agent attributes its performance drop to specific neighbor behaviors, the unexpected deceleration of vehicle 1 and the acceleration pattern of vehicle 3, and derives a targeted adjustment strategy.

Case 2 (Slow-down Scenario). The same agent position generated a qualitatively different signal:

“The spatial analysis indicates a general trend of deceleration, which may have influenced the need for a stronger deceleration to maintain formation.”

The agent attributes its adjustment to an aggregated mean-field spatial trend from unobservable agents, rather than to any individual neighbor’s behavior.

These two cases demonstrate fundamentally different attribution directions: Case 1 performs local neighbor-level attribution, while Case 2 reasons about collective spatial dynamics. This confirms that the Introspector adapts its diagnostic attribution analysis to the scenario’s underlying structure rather than applying a fixed reasoning pattern.

P.2 Quantitative Evidence: Diagnostic Attribution Statistics

To systematically evaluate whether the Introspector’s reflections constitute attribution reasoning, we analyzed three complete collaboration logs comprising all reflection instances across full simulation episodes. We clarify that the attribution explicitly references other agents’ behaviors, neighborhood statistical features, or inter-agent interaction effects as contributing factors to the observed performance change. Results show that 89.3% of reflections contain explicit attribution to other agents’ behaviors or neighborhood features, rather than self-trajectory patterns. This indicates that the Introspector systematically reasons about multi-agent interaction mechanisms rather than overfitting to local observation sequences.

P.3 Behavioral Coherence Verification

We further verify that the Introspector’s attribution reasoning translates into coherent behavioral adjustments. In the Catch-up case (Case 1 above), vehicle 2 identified that vehicle 1 decelerated unexpectedly (acceleration shifting from $+1.8$ to -1.3 m/s^2) while vehicle 3 maintained low acceleration. The diagnostic attribution concluded that stabilization was needed to prevent headway violation. Consequently, vehicle 2 adjusted its own acceleration from -1.05 to -0.82 m/s^2 , a conservative correction aligned with the diagnosed cause, reducing deceleration intensity to avoid over-correction given vehicle 1’s unexpected behavior.

This behavioral coherence, where the direction and magnitude of action adjustments logically follow from the attribution diagnosis, is further corroborated by the ablation results in Figs. 4 and 5, where removing the Introspector leads to persistent oscillations in CPP ($1.9\times$ degradation in RMSE-H) and 44.4% longer pandemic duration in PC, confirming that attribution adaptation is essential for long-horizon coordination.

Q Core Prompts of MACRO-LLM

Q.1 CoProposer

Fig. 8 provides the core prompts of proposal generation with a rollout-simulated verification in CoProposer.

Q.2 Negotiator

Fig. 9 provides the core prompts for proposal evaluation with spatial strategies and feature updates

in Negotiator when consensus is not achieved. Fig. 10 provides the core prompts for updating proposal with updated spatial strategies and features in Negotiator.

Q.3 Introspector

Fig. 11 presents the core prompts for generating the revision signal after completing one-step execution. Fig. 12 presents the core prompts for updating the temporal strategy using the drift intensity and semantic revision signal.

[*self-checking_rules*] are a set of rules for verifying the output format and common-sense consistency of LLM outputs. These rules ensure that the model correctly applies physical reasoning. For example, in CPP task, “If ACCELERATION_GAP > 0 , MY_VELOCITY will be INCREASED, MY_HEADWAY will be DECREASED.” These rules help correct occasional LLM mistakes, such as misjudging the travel direction of vehicles and thus misunderstanding how acceleration or deceleration affects inter-vehicle headway.

R AI Assistants in Writing

We utilized AI assistants (e.g., Gemini and Claude) exclusively for grammatical error correction, sentence polishing to enhance readability, and generating robot icons used in Figs. 1 and 2. We explicitly state that the core scientific concepts, experimental design, logical structure, reference, and substantive content of the paper were entirely human-authored without generative contributions from LLMs.



CoProposer: Proposal Generation Query

You are [agent_name] in a [task_name]. This is negotiation round 0 with your neighbors. Your task is to [task objective]. Decision-Making Steps (Follow strictly, step by step):

Step 0: Initial Decision for [agent_name] at the 1st time step, and define urgency of the action: Normal, Warning, Urgent.

Step 1: Collaborative acceleration for [observable_agents] to achieve objective with [Temporal Strategy], [Spatial Strategy] and [Spatial Features].

Step 2-4: Validation by 2 Time-Step Simulation: (time step 2 and time step 3).

Step 2: Simulate the next state (state_2) at time step 2. [instructions]

Step 3: Calculate collaborative actions for state_2.

Step 4: Simulate the next state (state_3) at time step 3. [instructions]

Step 5: Feasibility check for both state_2 and state_3

[task_constraints]

- If any constraint is violated, go back to Step 0 and pick a more conservative action. Repeat Steps 0-4 up to 10 times.
- If no feasible proposal is found after 10 iterations, output the best proposal found.

Output Format (STRICT):

```
<analysis>[analysis_and_calculation_steps] </analysis>
<proposal>[semantic_proposal_for_negotiation] </proposal>
<output>E[timestep]_R[round]_[agent_name]_proposal = {[my_name]: <proposed action for itself>,
[neighbor's_name]: <proposed acceleration for neighbor>}</output>
IMPORTANT: [self-checking_rules]
```

Figure 8: The core prompt of CoProposer.



Negotiator: Proposal Evaluation Query

You are [agent_name] for [task_name]. Your observable neighbor is [observable_agents]. In the last negotiation round, consensus was not reached. You need to analyze the disagreement and summarize your reasoning in the following steps:

Step 0: Analyze whether the strategy proposed by [agent_name] conflicts with the strategy proposed by its observable neighbors [agent_name]

[task_strategy_information]

Step 1: According to [Spatial Strategies] and [Spatial features], analyze whether the strategy proposed by [neighbors_agent] conflicts with the trends of [unobservable_agents].

[task_strategy_information]

Output as following format:

```
<deal>False</deal>
<reasons> Observable vehicles:[observable_agent_name] choose ..., and proposes .... It's strategy is match/conflict/not conflict with my strategy. The reason is ... I suggest it's weight in the range ...
[unobservable_agent_list]: They are strategy trend is match/conflict/not conflict with my strategy. The reason is ... I suggest it's weight in the range ...</reasons>
<spatial-strategy>[update_spatial_strategy]</spatial-strategy>
IMPORTANT: [self-checking_rules]
```

Figure 9: The core prompt of proposal evaluation and spatial strategy update.



CoProposer: Update Proposal

You are [agent_name]. This is the Round_[current_round] of [time_step]. Your observable states is [agent_name Observable State in time_step]. You need to update your proposal by following steps.

- **Case 1: If the flag between <deal></deal> is True, reuse the last proposal and output as following format:**

```
<analysis>(I will keep my last proposal, because ...)</analysis>
```

```
<proposal> [semantic_proposal_for_negotiation] </proposal>
```

```
<output>[structured_proposal_for_coding]</output>
```

Skip the following steps.

- **Case 2: If the flag between <deal></deal> is False:**

Step 1: Define the confidence weights for observable neighbors' proposal and unobservable vehicles weighted average acceleration. [weight_rules]

Output the confidence weights as following format:

```
<insights>neighbor_proposed_weight:<neighbor_proposed_weight value> unobservable_weight:
```

```
<unobservable_weight value> my_weight: <my_weight value></insights>
```

Step 2: Based on weights defined between <insights></insights>, weighted the proposed acceleration for each vehicles by following equations:

```
updated_acceleration = neighbor_proposed_weight * neighbor_proposed_acceleration + my_weight * my_acceleration + unobservable_weight * unobservable_trend.
```

/* Step 3: A rollout-simulated verification similar to Step 2-5 in CoProposer */

Output Format (STRICT):

```
<analysis>[analysis_and_calculation_steps] </analysis>
```

```
<proposal>[semantic_proposal_for_negotiation] </proposal>
```

```
<output>E[timestep]_R[round]_[agent_name]_proposal = {[agent_name]: <proposed action for itself>, [neighbor's_name]: <proposed acceleration for neighbor>}</output>
```

```
IMPORTANT: [self-checking_rules]
```

Figure 10: The core prompt of update proposal.



Introspector: Generate Semantic Revision Signal

You are [agent_name]. You can observe [observable_agent_name]. The total system reward for this time step is xx% lower than in the last time step indicating that the system state getting worse. Your individual reward has dropped from xx to xx, which drop xx%.

Step1. Based on [last_negotiation_record] and [this_negotiation_record], integrate the [Objective Instruction] to analyze whether the drop in episode reward was caused by yourself. If so, at which stage was responsible.

Infer whether the reward decline was caused by [observable_agents] or [unobservable_agents], and output between tags <reasons> </reasons>

Based on <reasons> </reasons> should strategies be adjusted to improve future episode rewards?

Step 1: You need to find out the rules that need to be adjusted based on the reasons you summarized.

Step 2: According to the related rules you summarized, be specific about "what to do" and "what to avoid" and output between tags <self-checking_rules> and </self-checking_rules>.

The output format as follows:

```
<reasons>[summarized_reasons]</reasons>
```

```
<self-checking_rules>(When states condition ... I need to/I need to avoid ...)</self-checking_rules>
```

```
IMPORTANT: [self-checking_rules]
```

Figure 11: The core prompt of generating semantic revision signal.



CoProposer: Update Strategy Query

You are [agent_name] to update its strategies. The total system reward for this time step is xx% lower than last time step, indicating that the system state getting worse. The overlap of transition (including state and action) among these two time steps is xx%, which means that their overall movement and decision patterns are xx% similar, with xx% differences in how the agent moves between states and selects actions.

Based on the <reasons></reasons> you summarized (from Fig. 11), update your strategies carefully with NO MORE than xx%.

Step 1. Calculate the change in state from the historical states to the current state and compare it to the previous temporal plan. Analyze if the change in state matches the plan of the previous temporal plan.

Step 2. Carefully check whether the change match the last temporal plan.

- If it matches, keep the original plan and update the temporal plan. Execute step 3 to return the updated plan.

- if it doesn't match, summarize the reasons and output within <reflect> tags as following: <reflect>(My final action does not match my original temporal plan, the reasons may be ...)</reflect>

According to the <reflect></reflect>, update the temporal plan.

Step 3. Output the updated plan with following format:

```
<temporal-strategy>[update_temporal_analysis]</temporal-strategy>
```

```
IMPORTANT: [self-checking_rules]
```

Figure 12: The core prompt of update strategy